processes

MDPI

Review

Mathematical Morphology-Based Fault Diagnosis for Rotating Machinery: A Review

Tingkai Gong [1], Xiaohui Yuan [2,*], Bing Ji [3] and Zhinong Li [4]

[1] School of Civil Aviation, Nanchang Hangkong University, Nanchang 330063, China; niattk@nchu.edu.cn
[2] School of Hydropower and Information Engineering, Huazhong University of Science and Technology, Wuhan 430074, China
[3] School of Traffic and Transportation Engineering, Central South University, Changsha 410075, China
[4] School of Instrument Science and Optoelectronic Engineering, Nanchang Hangkong University, Nanchang 330063, China
* Correspondence: yxh71@hust.edu.cn

Abstract

Rotating machinery is a crucial element of mechanical equipment, and during serving life, failures are inevitable due to human and non-human factors. Signal processing techniques serve as essential tools for diagnosing such faults. Among them, mathematical morphology (MM) has attracted considerable research interest in this domain owing to nonlinear filtering, simple computation rules and well-established theoretical foundation. Thus, numerous papers have been published in academic journals and conference proceedings. This review paper attempts to outline the morphological framework and to summarize these applications focusing on rolling element bearings and gears. Finally, it provides an analysis of the relevant discussions on MM, and suggests several potential prospects.

Keywords: mathematical morphology; morphological pattern spectrum; morphological wavelet; fault diagnosis; rotating machine; vibration signal

Check for updates

Academic Editors: Yifei Tong and Fengque Pei

Received: 6 December 2025
Revised: 9 February 2026
Accepted: 11 February 2026
Published: 13 February 2026

Copyright: © 2026 by the authors. Licensee MDPI, Basel, Switzerland. This article is an open access article distributed under the terms and conditions of the Creative Commons Attribution (CC BY) license.

1. Introduction

Rotating machinery is a significant component of modern industrial systems and plays a vital role in various applications. As a complex system, it comprises different rotating parts serving distinct functions; for example, bearings support axial and/or radial loads, while gears primarily transfer or modify speeds and motion directions. Typically, these rotating parts operate under harsh conditions, such as high temperature and pressure, as well as time-varying loads and speeds. Hence, the failure of rotating parts is inevitable, which compromises the reliability and operational effectiveness of the mechanical equipment. Therefore, condition monitoring of the mechanical systems, especially the key rotating parts, has become an efficient and available solution scheme in theoretical research and engineering practice [1,2].

Vibration measurement is particularly sensitive to the mechanical component faults, as it directly reflects the information associated with abnormal conditions. However, the acquired vibration signals are often non-stationary and nonlinear due to signal amplitude or/and frequency demodulation caused by time-varying operating conditions. Meanwhile, additive noise from background environment is embedded into such signals, which increases the difficulty of fault diagnosis. To address this issue, various signal processing methods are considered, such as short time Fourier transform (STFT) [3–7], wavelet analysis [8–12], empirical mode decomposition (EMD)-based method [13–17] and variational

mode decomposition (VMD) [18–23], etc. As we know, each of these methods has its own merits and demerits; for instance, STFT can simultaneously locate the change of interested signal components in time- and frequency-domains but cannot obtain the optimal resolution due to the Heisenberg uncertainty principle; EMD-based methods are operated without a predefined basis function and are suitable for processing non-stationary signals but suffer from mode mixing, end effect and noise sensitivity. VMD improves upon EMD but highly depends on the mode number and penalty coefficient.

Mathematical morphology is a robust and versatile theory. Firstly, it completes its extension from image processing to one-dimensional signal analysis. At the same time, the extension is further demonstrated through self-development and interdisciplinary integration. For example, self-development unifies qualitative and quantitative analysis for a specified target like fault diagnosis, while integration with other theories combines their respective merits. A classic example is morphological wavelet, which retains the nonlinearity of morphology and the multiresolution of wavelets. The robust framework is illustrated in Figure 1. As a result, morphological methods provide a multi-perspective framework for rotating machine fault diagnosis.

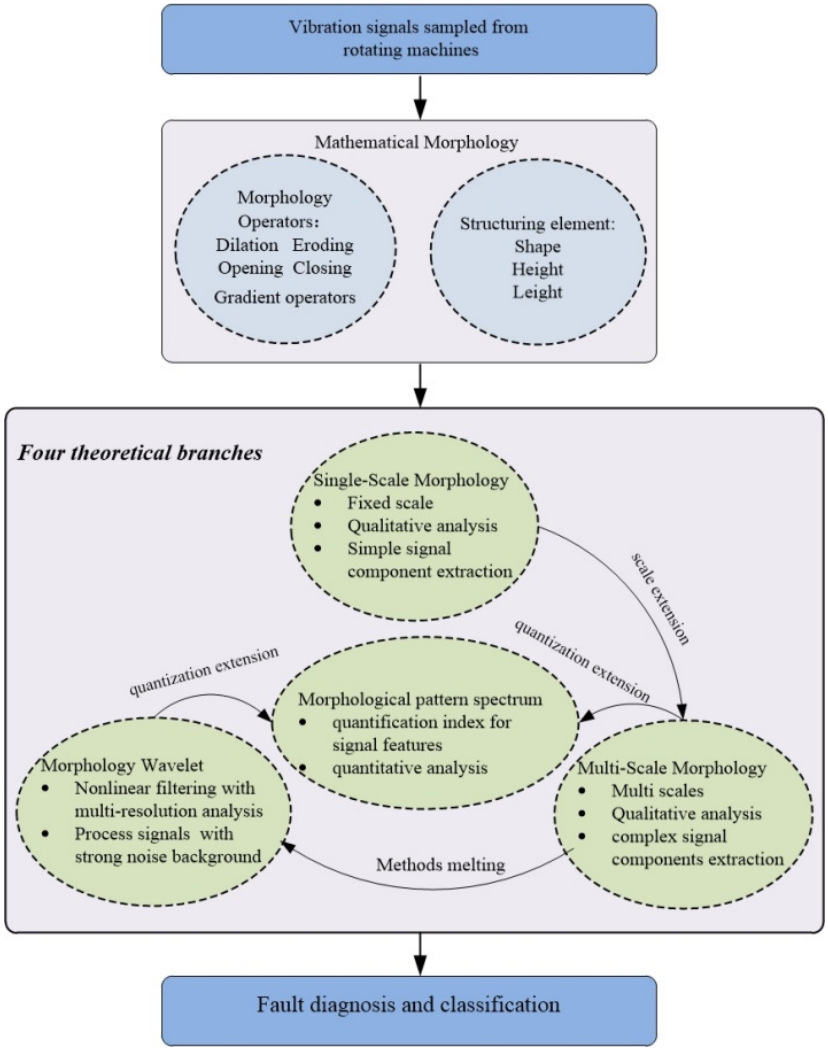


Figure 1. The framework to mathematical morphology.

Moreover, mathematical morphology is characterized by simple computation (i.e., addition, subtraction and local extrema solving), nonlinear filtering and strong signal demodulation ability; thus it has increasingly attracted wide attention in the rotating part

fault field, and enormous publications occur in academic journals, conference proceedings and technical reports. This paper makes an attempt to summarize and review the current studies, aiming to provide interested researchers with a clear and comprehensive overview of mathematical morphology. The remaining part of the paper is structured as follows. Section 2 presents morphological foundation about morphological operators, structuring elements and four morphology-based methods. Section 3 introduces the reference review on morphological applications in rotating machinery fault diagnosis, followed by a brief discussion on the rules of both operator selection and structuring element construction, and potential prospects in Section 4. Section 5 concerns the concluding remarks.

2. Mathematical Morphology

Morphological theory is developed based on set theory, topology, stochastic geometry, lattice theory, and nonlinear partial differential equations [24–26]. In the image processing field, it can complete image segmentation [27–31], image feature extraction [32–37], edge detection [38–41] and image enhancement [42–45]. Due to the nonlinear filtering and strong demodulation behavior of signal, it is gradually extended to 1D signal processing [46–48].

Mathematical morphology is an interaction between structuring element and a signal according to certain computational rules for removing irrelevant contents and retaining pivotal detail information. It involves two fundamental elements: morphology operator and structure element. The former defines the mathematical computation rules, whereas the latter works as an information carrier designed to extract targeted patterns from signals.

2.1. Morphological Operator

Morphology theory includes four basic operators, i.e., dilation, erosion, opening and closing. Let $f(n)$ be one-dimensional signal with a domain at $F = (0, 1, 2, \ldots, N-1)$, and $s(n)$ be a structuring element with at a domain at $S = (0, 1, 2, \ldots, M-1)$ ($M << N$). Then, dilation and erosion are formulated as

$$(f \oplus s)(n) = \max\{f(n-m) + s(n)\} \quad m \in 0, 1, 2 \cdots M-1 \tag{1}$$

$$(f \ominus s)(n) = \min\{f(n+m) - s(n)\} \quad m \in 0, 1, 2 \cdots M-1 \tag{2}$$

where $\oplus$ and $\ominus$ represent dilating and eroding, respectively. Because dilation and erosion correspond to addition and subtraction in arithmetic, they can expand or shrink the morphological shapes of images. It is noticed that in practical terms, the two operators cannot fully recover original image, thus closing and opening are defined as

$$(f \bullet \mathrm{s})(n) = (f \oplus \mathrm{s} \ominus \mathrm{s})(n) \tag{3}$$

$$(f \circ \mathrm{s})(n) = (f \ominus s \oplus s)(n) \tag{4}$$

where $\circ$ and $\bullet$ stand for opening and closing, respectively. Toward a one-dimensional signal, these operators have specified computation rules; for instance, dilation and erosion separately solve local max and minimum values. Based on Equations (3) and (4), closing firstly detects local maxima and then minima, and opening is an inverse performance.

On the other hand, these basic operators exhibit singular identification performance for the features of signal. In order to improve the situation, morphological gradient operators are constructed. For example, the difference between closing and opening (DCO) and the difference between dilation and erosion (DDE) are defined as follows:

$$DCO(f) = (f \oplus s \ominus s)(n) - (f \ominus s \oplus s)(n) \tag{5}$$

$$DDE(f) = (f \oplus s)(n) - (f \ominus s)(n) \tag{6}$$

In order to distinguish the signal feature extraction performance of these operators, simulation analysis is considered. Here, a linear flat SE with a length of 5 sampling points is employed. Figure 2a–f illustratethe signal feature extraction results of the six operators (i.e., dilation, erosion, closing, opening, and DDE and DCO, respectively. As shown, dilation smooths positive impulses while retaining negative ones, whereas erosion shows an inverse behavior. Similarly, closing extracts positive impulses and inhibits negative ones, whereas opening performs inversely. The gradient DDE embody certain random performance, whereas the gradient DCO retains the oscillatory trend of the simulated signals. It should be noted that the performance of these operators is highly dependent on both the computational rule of the used operator and the length of the defined SE.

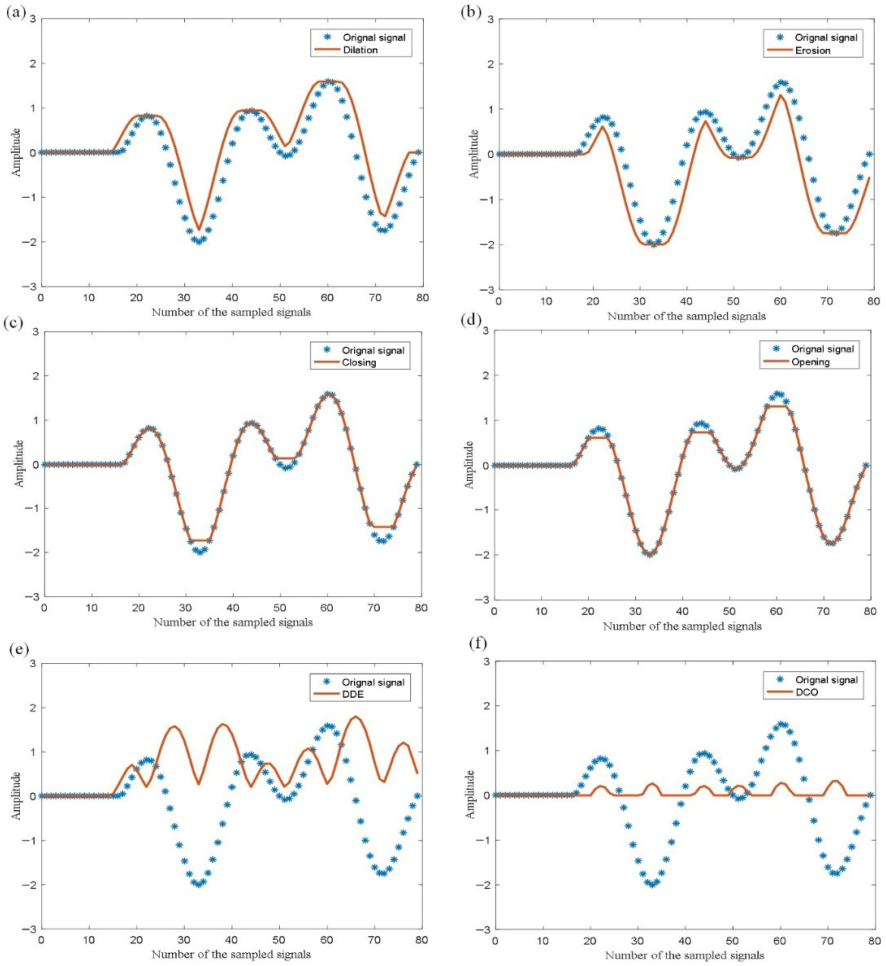


Figure 2. Performance of morphological operators to a simulated signal. (**a**) Dilation, (**b**) erosion, (**c**) closing, (**d**) opening, (**e**) DDE, and (**f**) DCO.

According to the analysis above, due to its simple computations, the change of signal in a local area can be easily understood when it is processed by mathematical morphology. Consequently, it provides a microcosmic and intuitive view to signal analysis, and brings more controllability in theoretical study and actual applications.

2.2. Structuring Element

Structuring element acts as a moving window to probe interested information in an original object. In other words, the structuring element is essentially a given information

carrier, and the morphological features in the object that are identical to the used SE can be extracted.

Compared with the original object, SE is simpler in shape and smaller in size, and comprises three physical properties: shape, length and height. The shape represents what geometric outline is concerned to us, and can be triangle, circle, disk, and rectangle, etc. In some cases, irregular shapes can also be defined. To a SE, the length and height parameters define its spatial scope of influence in the horizontal and vertical directions, respectively. Although it has three parameters, it does not mean that they all must be defined simultaneously. For example, height can be neglected, that is, defined as zero. According to this point, it is grouped into two types: flat structuring element and non-flat structuring element. The only difference between them is whether the height is involved in morphological operations. Figure 3 shows the difference when using dilation. When x_i in signal X is aligning with the underlined original of flat SE in Figure 3a, the dilation result is the max among x_{i-1}, x_i and x_{i+1}. Otherwise, it is the max among $x_{i-1} + h_0$, $x_i + h_1$, and $x_{i+1} + h_2$ in Figure 3b. On the other hand, if SE is {1 1 0}, the result is the max between the two points x_{i-1} and x_i, rather than the three points.

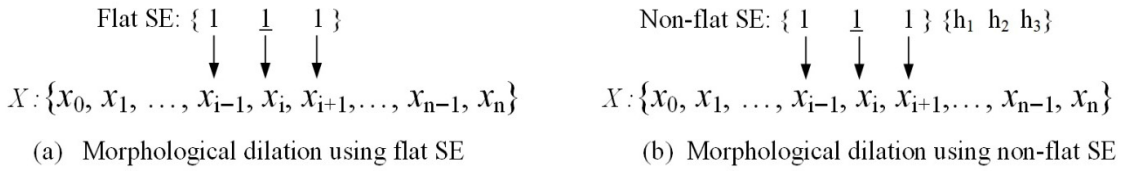


Figure 3. The difference between flat and non-flat SE when conducting dilation.

On the other hand, mathematical morphology is a nonlinear filter. As mentioned above, the length and height of the structuring element determine the computation range of morphological operations; namely, it primarily dominates the morphological filtering result. It can be concluded that a small SE is beneficial to preserve morphological features but unbeneficial to remove noise, and vice versa.

2.3. Introduction to Morphology-Based Methods

Mathematical morphology is a systematic theoretical framework. Four morphological methods frequently used in rotating machine fault diagnosis area are introduced, i.e., single-scale morphology (SSM), multi-scale morphology (MSM), morphological pattern spectrum (MPS) and morphological wavelet (MW).

2.3.1. Single-Scale Morphology

SSM means that just one structuring element is utilized in the morphology processing. In some cases, multiple SEs are used to obtain different morphological results, but the final result is eventually determined by an optimal SE produced through certain selection criterions, and it is still the analysis.

Relatively speaking, the single-scale analysis is simpler in applications; for instance, when flat SE is considered, the length only needs to be defined. As a result, its reasonability is quite crucial. Otherwise, the analysis easily suffers from under- or over-filtering. In general, SSM is suitable for processing the signals that do not contain multiple distinct signal components. This is because a single SE difficultly matches with the various morphology features in a complex signal. Consequently, an appropriate SE is the most vital factor for obtaining the desired result.

2.3.2. Multi-Scale Morphology

Multi-scale morphology is a comprehensive analysis, making it well suited for processing the complicated signals acquired from real environments.

In the multi-scale model, varying scales are achieved by self-dilation of a unit-scale SE. This method offers two advantages, enhancing computation efficiency and simplifying morphology calculation.

Let γ (γ = 1, 2, 3…γ_{max}) be the scale parameter, and s be a unit-scale SE. The SE at scale γ can be given as

$$\gamma s = \underbrace{s \oplus s \oplus \cdots s \oplus s}_{\gamma-1 \ times} \tag{7}$$

According to the definition above, the dilation and erosion of signal $f(x)$ at scale γ are written as

$$f \oplus \gamma s = \underbrace{f \oplus s \oplus \cdots s \oplus s(n)}_{\gamma-1 \ times} \tag{8}$$

$$f \ominus \gamma s = \underbrace{f \ominus s \ominus \cdots s \ominus s(n)}_{\gamma-1 \ times} \tag{9}$$

Also, the closing and opening of signal $f(x)$ at scale γ can be separately formulated as

$$f \cdot \gamma \mathrm{s} = \mathrm{f} \oplus \gamma \mathrm{s} \ominus \gamma \mathrm{s}(\mathrm{n}) \tag{10}$$

$$f \circ \gamma s = f \ominus \gamma s \oplus \gamma s(n) \tag{11}$$

Similarly, morphological gradient operators DCO and DDE at scale γ are represented as

$$DCO(f)_{\gamma} = (f \cdot \gamma s)(n) - (f \circ \gamma s)(n) \tag{12}$$

$$DDE(f)_{\gamma} = (f \oplus \gamma s)(n) - (f \ominus \gamma s)(n) \tag{13}$$

In multi-scale analysis, the used scales are generally continuous. At the same time, small scales are beneficial to retain signal features but are less effective for noise removal; thus, the scales must be properly defined, otherwise over- or under-analysis is produced.

2.3.3. Morphological Pattern Spectrum

In image processing, shape representation and shape-size description are two key tasks, because the former qualitatively identifies that what important information an image contains, while the latter quantitatively measures how much of such information is present in the image. However, SSM and MSM merely determine whether a structural element is contained within the image; thus, they are essentially qualitative analyses. In fact, quantifying specific image information allows for more accurate estimation and deeper understanding for an image; thereby, Maragos presented a morphological pattern spectrum [49,50], which is also called granulometric measurement [51–54].

In fact, there are some relativities between MPS and Fourier transform (FT). As we know, the FT of a signal $f(t)$ is written as $F(\omega) = \int_{-\infty}^{\infty} f(t)e^{-i\omega t}dt$, noticing that the spectral component is calculated through a modulation $f(t)e^{-i\omega t}$, when the frequency ω is defined, the spectral component is obtained by measuring the area of the modulation. Varying ω over a given interval, the frequency spectrum of the signal can be produced. Obviously, complex signal $e^{-i\omega t}$ works as a probing pattern with a series of spectrum component ω, and they can be extracted by the interactions between the complex signal and a given signal.

According to similar consideration, solving the area of an image X by morphology operations is defined here. Firstly, it uses a structuring element S_n, where subscript n

defines S as a specified shape with a certain size r. When X is processed by opening operation with S_n, the area of the transformed image is calculated as

$$F(r) = A(X \circ rS)/A(X) \tag{14}$$

where notation $A(\bullet)$ means area solving, and numerator and denominator stand for the areas of opening and the original image X, respectively. Because the area of image $A(X)$ is fixed and the area $A(X \circ rS)$ varies with the change of r, the function $F(r)$ represents the probabilistic measures of the size distribution relate to S of size r in an image.

Based on the area measurement above, MPS can be defined as differential size distribution:

$$MPS_X(r, S) = -dA(X \circ \mathrm{rS})/dr \quad r \geq 0 \tag{15}$$

It represents the union that contains all patterns of X that are relative to a special size r. Furthermore, by varying S or r, different types of information can be extracted. For example, if S is defined with different geometric shapes while keeping r fixed, the MPS indicates which shape the image most closely resembles. If r changes while keeping S fixed, it obtains the distribution of S across different scales within the image. Additionally, Convexity of S implies that MPS is non-negative for all $r \in R$ due to $X \circ rS \supseteq X \circ lS$ if $r \leq l$; thus, MPS is the non-negativity when increasing r.

Correspondingly, when a closing operator is used, MPS is written as

$$MPS_X(-\gamma, s) = dA(X \cdot rs)/dr \quad r > 0 \tag{16}$$

In image processing, the positive scale refers to processing the umbra of an image, while the negative scale refers to processing its complementary. Because size r in Equation (16) is continuous, it is difficult to use an analytical way to compute MPS. Accordingly, the discrete MPS is given as

$$MPS_f(+n, s) = A[f \circ ns - f \circ (n+1)s] \quad 0 \leq n \leq N \tag{17}$$

$$MPS_f(-n, s) = A[f \cdot ns - f \cdot (n-1)s] \quad 1 \leq n \leq K \tag{18}$$

where N and K are the maximum and minimum size n, respectively, and $A(f)$ is calculated as the difference between the results of opening (or closing) operations at adjacent scales.

Morphology pattern spectrum is a quantitative model based on a multi-scale and shape-driven tool. Depending on varying the shape of SE and its scale r, it can quantify the morphological features of an object. Therefore, MPS offers a potential technique combining signal processing with feature quantification.

2.3.4. Morphological Wavelet

In the real world, the features of signals vary over both scale- and resolution-domains and present highly non-stationary in space. Researchers have recognized that multiresolution signal decomposition is fairly significant for both theoretical development and practical applications, because it makes these features represented across different scales, thereby providing an efficient and clear interpretation of such signals with considerable computational advantages.

As a classical multiresolution technique, traditional wavelet transforms (TWTs) termed first-generation wavelets, relies on Fourier transform and z transform to design a filter bank with special properties intrinsically aligned with the multiresolution analysis. This approach has been widely used in signal and image processing applications [8–12]. Obviously, TWT is a linear method like signal scaling, but it is may not be compatible with

attributes of interest, for example, blurring the edge information of a signal. Hence, scholars made contributions to extend multiresolution analysis from linear to nonlinear frameworks, expecting that the obtained results would vary in a non-intuitive manner.

The extension should involve two aspects: non-redundant to signal decomposition and perfect reconstruction to signal reconstruction. To satisfy the requirements, it experiences many trials. In 1991, Pei and Chen [55,56] firstly put forward non-redundant nonlinear sub-band decomposition using morphological theory, but it cannot perform perfect signal reconstruction. For this reason, Egger and Li [57] developed an improved method by means of median-type operation, and a similar study is found in the literature [58]. Subsequently, Queiroz et al. [59] proposed a type of nonlinear wavelet decomposition for lowering image code complexity. In 1997, Cha and Luis [60] used a morphological opening operator to construct a nonlinear wavelet transform with perfect signal reconstruction.

During the extension process, these studies provide significant reference for future development, but do not present a general framework in morphology area to such nonlinear development. Differently, the traditional wavelet is done well at the same period, i.e., lifting scheme termed second-generation wavelet [61–63].

Inspired by the lifting scheme, Goustias and Heijmans [64,65] proposed an axiomatic framework morphological wavelet, which presents two wavelet-type decompositions: a nonlinear scheme called coupled wavelet decomposition and a linear one called uncoupled wavelet decomposition.

1. Coupled wavelet decomposition

To nonlinear signal decomposition cases, coupled wavelet decomposition is conducted by three operators: two analytical operators (one for the approximation signal and another for the detail signal) to perform multiresolution analysis and one synthesis operator to reconstruct signal.

Assume that V_j and W_j are signal space and detail space at level j, respectively. Then, the signal decomposition is performed by analytical operators as increased direction through mapping level j into $j + 1$, i.e., the analysis operator $\psi_j^{\uparrow} : V_j \longrightarrow V_{j+1}$, and the detail operator $\omega_j^{\uparrow} : V_j \longrightarrow W_{j+1}$. The analysis operator can obtain approximation or simplification of signal with many signal properties, while the detailed operator can capture localized morphological features. Reversely, the synthesized operator is conducted as decreased direction $\Psi_j^{\downarrow} : V_{j+1} \times W_{j+1} \longrightarrow V_j$. The one-stage decomposition is depicted in Figure 4a.

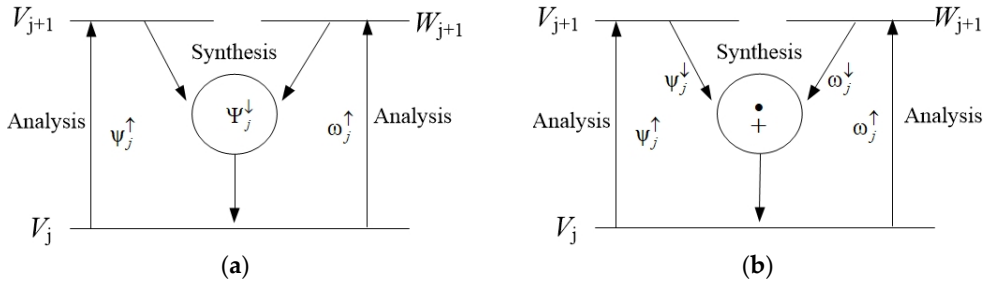


Figure 4. (**a**) Coupled wavelet decomposition scheme. (**b**) Uncoupled wavelet decomposition scheme.

On the other hand, when Equations (19) and (20) are held, the robust signal decomposition method guarantees the non-redundancy in decomposition and the perfection in reconstruction. At the same time, the two conditions implicitly show that the mapping of operators is injective upward and surjective downward.

$$\Psi_j^{\downarrow}\left(\psi_j^{\uparrow}(x),\ \omega_j^{\uparrow}(x)\right) = x,\ if\ \mathrm{x} \in V_j \tag{19}$$

$$\begin{cases} \psi_j^{\uparrow}\left(\Psi_j^{\downarrow}(x,y)\right) = x, \ if \ x \in V_{j+1}, y \in W_{j+1} \\ \omega_j^{\uparrow}\left(\Psi_j^{\downarrow}(x,y)\right) = y, \ if \ x \in V_{j+1}, y \in W_{j+1} \end{cases} \tag{20}$$

According to the decomposition scheme, a given signal $x_0 \in V_0$ can be decomposed in the recursive way as

$$x_0 \to \{x_0, y_0\} \to \{x_1, y_1\} \to \{x_2, y_2, y_1\} \to \cdots \{x_k, y_k, y_{k-1}, \cdots y_1\} \to \cdots \tag{21}$$

On the other hand, the original signal can be completely rebuilt from sub-signals x_{k} and y_1, $y_2, \cdots y_k$ by the synthesized scheme:

$$x_j \ = \ \Psi_j^{\downarrow}(x_{j+1}, y_{j+1}), \quad j \ = \ k-1, k-2, \cdots 0 \tag{22}$$

Hence, the signal decomposition scheme as Equations (19)–(21) is called the coupled wavelet decomposition scheme.

2. Uncoupled wavelet decomposition

In a morphological wavelet, the uncoupled wavelet scheme is a linear decomposition as a special case of the nonlinear decomposition, and the decomposition procedure is similar to that of the nonlinear one. The signal synthetization uses a binary addition operation $\dot{+}$ to make Equation (23) hold when $\psi_j^{\downarrow} : V_{j+1} \longrightarrow V_j$ and $\omega_j^{\downarrow} : W_{j+1} \longrightarrow V_j$. The two operators $\psi_j^{\downarrow}$ and $\omega_j^{\downarrow}$ are taken to the signal synthesizing and the detail synthesizing, respectively.

$$\Psi_j^{\downarrow}(x,y) = \psi_j^{\downarrow}(x) \dot{+} \ \omega_j^{\downarrow}(x) \quad x \in V_{j+1}, y \in W_{j+1} \tag{23}$$

Meanwhile, satisfying Equation (24) ensures perfect signal reconstruction. Similarly, satisfying both Equations (25) and (26) guarantees non-redundant signal decomposition.

$$\psi_j^{\downarrow}\psi_j^{\uparrow}(x) \dot{+} \ \omega_j^{\downarrow}\omega_j^{\uparrow}(x) = x, \quad if \ x \in V_j \tag{24}$$

$$\psi_j^{\uparrow}\left(\psi_j^{\downarrow}(x) \dot{+} \ \omega_j^{\downarrow}(x)\right) = x, \quad if \ x \in V_{j+1}, y \in W_{j+1} \tag{25}$$

$$\omega_j^{\uparrow}\left(\psi_j^{\downarrow}(x) \dot{+} \ \omega_j^{\downarrow}(x)\right) = y, \quad if \ x \in V_{j+1}, y \in W_{j+1} \tag{26}$$

For a signal $x_0 \in V_0$, the reconstruction in a recursive synthesis scheme is given as Equation (27).

$$x_j = \psi_j^{\downarrow}(x_{j+1}) \dot{+} \ \omega_j^{\downarrow}(y_{j+1}) \quad j = k-1, \ k-2, \ \cdots, \ 1, \ 0 \tag{27}$$

This indicates that the signal x_j at level j can be reconstructed as mapping-down by the standard addition of the approximation signal and the detail signal at level $j + 1$. As a result, the signal representation process represented as Equations (21)–(25) is the uncoupled wavelet decomposition scheme. It is illustrated in Figure 4b.

Morphological wavelet achieves a nonlinear extension of TWT by incorporating mathematical morphology, keeping the multiresolution analysis and retaining shape and edge features. It provides a flexible and versatile method for signal analysis.

3. Application of Mathematical Morphology to Rotating Machine Fault Diagnosis

Aiming at bearing and gear fault diagnosis, the morphology-based approaches have conducted many theoretical developments and achieved successful applications. This section presents a synthetical summary on rotating machinery fault diagnosis, with clas-

sifications of single-scale morphology, multi-scale morphology, morphological pattern spectrum and morphological wavelet.

3.1. Single-Scale Morphology-Based Rotating Parts Fault Diagnosis

SSM just uses an operator with a SE to complete a morphological operation and is relatively simple in practical applications. Under the condition, the morphology filtering behavior highly relies on the physical properties of the structuring element.

3.1.1. SSM to Detect Bearing Defects

Nikolaou and Antoniadis [66] firstly employed SSM to extract the impulsive signals from defective bearings. They analyzed the different properties of morphology operators of impulsive signals and experimentally defined a flat structure element length. Huang et al. [67] constructed a dynamic model for the outer race of rolling bearing, and used a morphological filtering with the flat SE of the length of 120 sampling points to remove the noisy signals of the vibration signal produced by the model. The similar method that empirically selects the SE length is founded in Refs. [68–71] when diagnosing bearing failure. In this case, the sampling frequency of raw signals and the noisy interference intensity all affect morphological results, easily resulting in over- or under-filtering phenomena.

In order to deal with the problem, many scholars attempt to utilize some adaptive methods to construct SE. For instance, Yu et al. [72] defined the optimal length, i.e., when the amplitude of the first five feature frequencies of bearings is largest. Hu et al. [73] presented the SE construction method according to the relationship between the bearing fault impulse and a harmonic function with the resonant frequency, and harmonic waveform in a period.

In addition, optimization algorithms are also employed to obtain the optimal SE length. For example, Yan and Jia [74] presented a morphological slice bispectrum fused with cuckoo searching for diagnosing bearing failure. Van et al. [75] used a particle swarm optimization algorithm to obtain the SE length. Liu et al. [76] proposed a group spare balanced morphological filtering for detecting bearing compound faults. In the study, the WOA algorithm is considered to define the optimal SE length. Zhou et al. [77] used the PSO method to define the length and height parameters of a sinusoidal SE when diagnosing spindle motor bearing faults.

On the other hand, when morphology filtering is implemented using structural elements of various lengths, the filtered signals show distinct statistical properties in the time, frequency, or time–frequency domains. Consequently, special evaluation metrics are considered to determine the optimal SE length. Li et al. [78] and Wang et al. [79] presented a characteristic frequency intensity coefficient as the index to select the optimal length of SE. Zhang et al. [80] calculated alpha stable distribution to optimize the flat SE length and demonstrated the optimization superiority in capturing bearing outer and inner fault characteristic frequencies when compared with the optimization based on kurtosis. Noting that the aforementioned studies only employed one indictor to define the structuring element length, considering the higher reliability, some researchers tend to use a combination between multiple indicators to achieve the task. For instance, Wang et al. [81] proposed combining feature energy factor with permutation entropy to set the SE length when extracting bearing fault features. Lv et al. [82] designed a fusion indicator separately based on kurtosis and Renyi entropy, and kurtosis and Teager energy operator to select the optimal SE length, and the results demonstrated that it is effective and robust to incipient bearing fault detection. Li et al. [83,84] employed a characteristic frequency intensity coefficient in conjunction with third-order cumulant slice spectrum and diagonal slice spectrum to define the SE length for bearing fault feature extraction.

3.1.2. SSM to Detect Gear Defects

Feng et al. [85] applied four sampling points as the SE length in SSM to filter background noise from raw signals and calculated multi-fractal entropy to classify gear working statuses. Zhou et al. [86] empirically defined the linear SE length to demodulate the gear fault features. Yu et al. [87] proposed a gear fault diagnosis method-based Dual-Tree Complex Wavelet Packet and mathematical Morphology with the SE of a fixed length.

Bo et al. [88] developed a hybrid approach based on morphological filtering, wavelet theory and empirical mode decomposition to detect the incipient gear fault. Guo et al. [89] presented a combined scheme based on single-scale morphology, where the optimal SE length is adaptively determined according to kurtosis and modulation signal bispectrum.

3.2. Multi-Scale Morphology-Based Rotating Parts Fault Diagnosis

MSM acts as an extension to SSM; thus, it is more suitable for handling complex real signals. Essentially speaking, the multi-scale analysis still considers establishing the corresponding relationship between the SE scales and the morphological feature of a signal. As a result, the effectiveness of MSM also depends on the reasonability of the used scales.

3.2.1. MSM to Detect Bearing Defects

Feng et al. [90] considered a hybrid scheme based on MSM and manifold learning to classify bearing flaws. Gong et al. [91] proposed a repeated multi-scale morphology to deal with surplus noise at some small scales after conventional multi-scale analysis. Refs [92,93] defined the SE scales from unit scale to 0.6 times impulse period when extracting bearing fault feature frequencies. Gong et al. [94] introduced an iterative asymmetric multi-scale morphology for the amplitude demodulation of vibration signatures of defective bearings.

The scale definition in Refs. [90–94] is an empirical way. In order to adaptively define the SE scale, Li et al. [95] proposed the final scale as $f_s/f - 2$, where f_s is the sampling frequency of bearing vibration signals, and f is bearing fault feature frequency. The same method is found in Refs. [96–99]. Wang et al. [100] presented a planet-bearing fault diagnosis approach based on stochastic resonance and mathematical filtering, in which the scales are defined by a cloud genetic algorithm. Zhang et al. [101] considered a multi-scale scheme, where the length and height scales of non-flat SE are defined by the local minimum points in the vibration signals sampled from faulty bearing. In the same way, Li et al. [102] presented the scale definition based on local extrema to detect bearing characteristic frequency and its harmonic. Yao et al. [103] constructed a scale-adaptive tool using mathematical morphology spectrum entropy for evaluating bearing performance degradation. Shuai et al. [104] designed a local-peak-interval scale definition with support vector regression to distinguish roller bearing fault types. Cui et al. [105] presented an information-entropy threshold to obtain optimal scales. Duan et al. [106] and Tang et al. [107] presented the multi-scale morphological filter using cut-off frequency to define the SE scales for bearing fault feature extraction. Deng et al. [108] studied particle swarm method to optimize the weight of each scale in the reconstructed signals, and finally roller bearing fault diagnosis performance is improved. Yan et al. [109] presented a scale definition method based on bearing feature frequencies.

Generally speaking, when a SE with a specified scale is set, it will scan a given signal from the first point to the last one. Differently, Wang et al. [110,111] proposed a novel structuring element scale definition in a more microcosmic way, in which the shape and length of the SE is specified based on local minima in the adjacent waveforms of a signal. Furthermore, such a SE is just used in a local area, without the traditional time-shifting in the signal.

3.2.2. MSM to Detect Gear Defects

Ye et al. [112,113] employed multi-scale morphological filtering combined with intelligent algorithm for classifying gear pitting tooth, crack tooth and worn tooth with different levels. Guo et al. [114] defined the range of flat SE scale base on the signal sampling frequency and gear fault feature frequency to diagnose sun gear chipping in a planet gearbox. Wang et al. [115] utilized a multi-scale analysis using three fixed scales for diagnosing the gearbox faults. When facing gearbox defect recognizing, Cai et al. [116] defined the SE scales as the method in Ref. [96].

In order to adaptively define the scales, Refs. [117–119] used the adaptive scale definition method in Ref. [101] to discriminate gearbox faults. Zhang et al. [120] and Yu et al. [121] developed a multi-scale morphology to diagnose gear fault, where the SE scales are chosen adaptively based on kurtosis. Liu et al. [122] proposed a scale optimization method based on the parameter changing of impact signals for locating gear faults. Yan et al. [123] constructed a special indictor melting signal-to-noise ratio with fault feature ration to choose the SE scales when identifying wind turbine gearbox faults. Liu et al. [124] employed Chebyshev window as structuring elements, and defined the length and height scales based on the signal features of a planetary gearbox. Zhuang et al. [125] proposed the back-propagation learning algorithm to update the SE scale for detecting gearbox failure. In order to remove impulse interference of the vibration signals of gearbox, Cao et al. [126] designed the SE length selection as the maximizing L-kurtosis method.

3.3. Morphological Pattern Spectrum-Based Rotating Parts Fault Diagnosis

Unlike SSM and MSM, MPS establishes a one-to-one mapping relationship between the quantifiable spectrum indices and the defined patterns, and it is able to distinguish the operating statues of rotating parts under different working conditions.

3.3.1. MPS to Detect Bearing Defects

Chen et al. [127] calculated morphological pattern spectrum as the inputs of an improved support vector machine (SVM) algorithm to classify the outer fault, the inner race fault, and the ball fault on rolling ball bearing. In order to improve bearing fault classification accuracy, Gao et al. [128] proposed an optimized method based on MPS and S transform to bearing faults, and found that it can distinguish normal state and abnormal state with three fault levels. Sun et al. [129] calculated morphological pattern spectrum obtained by dilation as the inputs of support vector machine to classify bearing faults. Zhu et al. [130] noticed that in the vibration signals of defective bearings, the detailed features are similar but vary in their temporal positions. They introduced a hit-and-miss feature vector defined at local impact positions to enhance the recognition performance of classifier. Li et al. [131] calculated MPS using the difference between opening and closing, and used a least square support vector machine to recognize different wheelset bearing fault types. Gao et al. [132] developed the MPS of the time–frequency representations of signal as the input feature vectors of the classifier to identify bearing states.

Those investigations mentioned above are applications on basic MPS. In fact, morphology pattern spectrum can be further developed to special targets. For example, Hao et al. [133,134] believed that the combination between MPS entropy and barycenter scale location of spectrum is more effective than the combination between kurtosis and enveloping demodulating spectrum when differentiating six bearing defects. Wang et al. [135] noticed that an original MPS cannot recognize between damaged and normal bearings. They therefore introduced the sample entropy and Lempel–Ziv complexity of an MPS curve as a bearing fault classification index. Yu et al. [136] developed MPS entropy and pattern spectrum values as feature parameters of a proximal SVM for bearing fault classi-

fication. Yan et al. [137] exploited a multi-scale pattern gradient spectrum entropy based on MPS as the input feature sets of extreme machine learning, with experimental results demonstrating its effectiveness in bearing defect classification.

MPS works not only as a tool for bearing fault classification, but also as an indicator for bearing performance assessment. For instance, Zhao et al. [138,139] presented a new idea entitled high-order differential morphological spectrum entropy based on MPS and applied it to bearing performance trend prediction. Li et al. [140] extended the conventional definition of MPS to a generalized space, and both simulation and practical applications demonstrated its effectiveness in evaluating bearing performance. Gao et al. [141] observed that it has a strong relationship between generalized pattern spectrum entropy and bearing performance degradation course, Similarly, Wang et al. [142] found that the improved MPS entropy exhibits a consistent and perfect correlation with bearing degradation degree.

3.3.2. MPS to Detect Gear Defects

Li et al. [143] constructed morphological pattern spectra derived separately from four basic operators as the inputs of a K nearest neighbor classifier, a Bayes classifier and a least-square support vector machine. The results indicated that the MPS obtained by erosion performed best for gear fault classification. Li et al. [144] characterized the time–frequency representation based on S transform by morphological pattern spectrum to recognize five gear states. Barbieri [145] applied correlation analysis to compare MPS of signals sampled from different gear states, and integrated it with wavelet transform, single value decomposition, and stabilization diagram to discriminate the defects in gear and bearing installed in a gearbox.

3.4. Morphological Wavelet-Based Rotating Parts Fault Diagnosis

Morphological wavelet is a nonlinear multiresolution signal decomposition scheme, with high computation efficiency and superior ability to retain local signal features. It is capable of providing a distinct analytical perspective for rotating-part defect diagnosis.

3.4.1. MW to Detect Bearing Defects

Wang et al. [146] designed a mixed scheme combining lifting morphological wavelet with ensemble empirical mode decomposition for extracting fault features of defective rolling element bearings. Li et al. [147] proposed an adaptive morphological gradient lifting wavelet, in which an average filter and a morphological gradient filter were used to update the approximating signal, and the results showed that the proposed algorithm outperforms linear wavelet transform in bearing fault diagnosis. Li et al. [148] analyzed the geometrical structures of the bearing vibrations across various morphological scales, and developed a morphological stationary wavelet to extract bearing fault features. Chen et al. [149] performed a MW decomposition method based on open and closing operators for impulse feature extraction of damaged bearings.

Hao et al. [150] proposed a novel morphological undecimated wavelet decomposition scheme for bearing defects, and found that this scheme outperforms enveloping demodulation analysis and the traditional wavelet transform. Meng et al. [151] used a morphological wavelet and morphological filter to diagnose the outer, inner and rolling ball faults and the mixed bearing faults. Khakipour et al. [152] performed a morphological wavelet based on a morphology gradient operator to detect bearing flaws and demonstrated its superiority by comparing with a morphological Harr wavelet and the morphological undecimated wavelet decomposition. Li et al. [153] focused on an undecimated MW lifting scheme based on a morphological convolution operator to identify bearing defects. Guo et al. [154] integrated a morphological undecimated wavelet with morphological filtering to extract the weak fault features of rolling bearing. Li et al. [155] employed the different morphology

operators in a morphological undecimated wavelet to effectively suppress noisy signals, and the experimental results indicated that it accurately diagnoses the wheelset bearing compound faults.

Li et al. [156] took full advantage of the nonlinear characteristics of morphology Harr wavelet, and combined it with Perona–Malik filtering to detect the bearing inner race failure. Duan et al. [157] employed an empirical morphology undecimated wavelet to process the faulty bearing vibration signals, and demonstrated its effectiveness in fault diagnosis with high computation efficiency. In addition, Wang et al. [158] presented a morphological undecimated wavelet scheme, in which an improved gradient based on closing and opening is used as an analysis operator, and showed that the improvement can avoid statistic bias in faulty bearing vibrations analysis.

Zhang et al. [159] proposed using the combination of dilation and erosion as a synthesis operator and the combination of opening and closing as an analysis operator, and the results demonstrated that the undecimated decomposition is well suited for bearing fault diagnosis. Yong et al. [160] constructed a morphological wavelet package decomposition method, then used a soft threshold to remove the noisy signals for bearing fault feature detection. Yang et al. [161] presented an integrated approach based on morphological wavelet and S transform, demonstrating that MW can inhibit noise and the harmonic components related to axis rotating frequency, thereby enhancing bearing fault diagnosis performance.

3.4.2. MW to Detect Gear Defects

Liu et al. [162] used a morphological gradient wavelet to remove the noisy signals of gear fault, and the spectral graphs generated by multi-scale S transform to detect gear defects. Li et al. [163] utilized morphological gradient wavelet to detect gear fault feature frequencies. Zhang et al. [164] presented a multi-scale morphological undecimated wavelet decomposition combined with grey incidence analysis to identify gear fault patterns. Hong et al. [165] employed morphological mean wavelet transform to gear fault diagnosis, noting its sensitivity to local signal extrema and its effectiveness in noise reduction. Zhang et al. [166] developed a morphological Harr wavelet to process raw signals and used permutation entropy as a fault eigenvalue for detecting various gear fault types. Cai et al. [167] proposed a morphological wavelet method to cancel the strong noisy signals when diagnosing gear fault. Ding et al. [168] introduced a morphological Harr wavelet to purify the vibration signals from faulty gearboxes and used Permutation entropy for fault type classification. Zhang et al. [169] developed a max-lifting morphological wavelet for extracting gear features, in which dilation is used as both as a predicted and updated operator.

Tong et al. [170] employed a weighted morphological undecimated wavelet decomposition along with correlated kurtosis to gear defects. Shen et al. [171] found that morphological wavelet denoising is effective in extracting gear fault features. Li et al. [172] observed that the traditional morphological wavelets are limited in handling the sudden impulses from damaged gears due to their usage of fixed filters, and consequently proposed an adaptive morphological undated lifting wavelet.

3.5. Morphology-Based Methods for Other Mechanical Defective Objects

Li et al. [173] investigated an adaptive multi-scale morphology to recognize railway wheel flat, in which the optimal scales are defined by spectrum kurtosis criterion. Jiang et al. [174] proposed a hybrid method based on local mean decomposition and adaptive multi-scale morphology to demodulate the defective hydraulic pump signals, and believed that it exhibits strong noise resistance and demodulation abilities. Li et al. [175] introduced an improved morphological pattern spectrum into time–frequency analysis and the results illustrated that this approach is effective to characterize the vibration features from an

engine under five operating states. Qiu et al. [176] firstly defined the scale of flat SE in the range from unit scale to scale 100, and determined the optimal one by power spectral entropy and feature energy ratio for diagnosing axial piston pump fault.

3.6. Analysis of Operators and SE in Applications

These representative applications summarized in Table 1 demonstrate the applicability and robustness of mathematical morphology in the rotating machine fault diagnosis. Meanwhile, it is also notable that the existing research primarily focuses on two aspects: the morphological operator and the structuring element, both of which contribute to enhancing the morphology performance in practice, but the latter is dominates. Therefore, we further analyze the selection of morphological operators and the definition of the structuring element.

Table 1. Summarization of rotating components using the morphology-based method.

Object	Ref.	Method
Bearing	Nakolaou [66], Huang [67], Chen [68], Jiang [69], Duan [70], Meng [71], Yu [72], Hu [73], Yan [74], Van [75], Liu [76], Zhou [77], Li [78], Wang [79], Zhang [80], Wang [81], Lv 82], Li [83,84]	SSM
	Feng [90], Gong [91], Lv [92], Tang [93], Gong [94], Li [95], Yan [96], Qu [97], Yu [98], Li [99], Wang [100], Zhang 101], Li [102], Yao [103], Shuai [104], Cui [105], Duan [106], Tang [107], Deng [108], Yan [109], Wang [110,111]	MSM
	Chen [127], Gao [128], Sun [129], Zhu [130], Li [131], Gao [132], Hao [133,134], Wang [135], Yu [136], Yan [137], Zhao [138,139], Li [140], Gao [141], Wang [142]	MPS
	Wang [146], Li [147], Li [148], Chen [149], Hao [150], Meng [151], Khakipour [152], Li [153], Guo [154], Li [155], Li [156], Duan [157], Wang [158], Zhang [159], Yong [160], Yang [161]	MW
Gear	Feng [85], Zhou [86], Yu [87], Bo [88], Guo [89]	SSM
	Ye [112,113], Guo [114], Wang [115], Cai [116], Li [117], Wei [118], Luo [119], Zhang [120], Yu [121], Liu [122], Yan [123], Liu [124], Zhuang [125], Cao [126]	MSM
	Li [143], Li [144], Barbieri [145]	MPS
	Liu [162], Li [163], Zhang [164], Hong [165], Zhang [166], Cai [167], Ding [168], Zhang [169], Tong [170], Shen [171], Li [172]	MW
Others	Li [173], Jiang [174]	MSM
	Li [175], Qiu [176]	MPS

3.6.1. Morphological Operator Selection

The morphological operator determinates the rules of the morphological operation, determining which type of morphological feature in a signal can be recognized. In this field, operators are generally categorized into three classes: basic operators, gradient operators, and product operators. There are some recommendations for operator selection in engineering applications.

Basic operators have single morphology processing, i.e., they can extract one type of signal morphological features; for example, closing can just detect the positive impulses of a signal. Therefore, it is suitable for dealing with the vibration signals of a rotating machine in a laboratory environment. When facing complex working conditions like strong nonlinear superposition between signals, it easily results in information loss.

Gradient operators can cancel the shortcoming of basic operators, enhancing filtering performance and retaining much more signal features. As a result, it is applicable to diagnosing bearing and gear defects under complex conditions, where original vibration signals typically exhibit strong impulsive distortion and cover noise at a moderate level.

Several novel operators constructed by the product of basic operators [77,80,99] can stress the amplitude difference of vibration signals with many more features extracted and inhibit the random fluctuation of noise. As a result, it is suitable for scenarios such as strong noise interference and weak signal features, especially for the diagnosis of incipient bearing and gear faults. In nature, the product can amplify the weak characteristics and is robust to noise.

In a word, for the operator selection, basic ones are used for coarse filtering. If it needs better diagnosis performance, gradient operators should be considered. Under complex conditions with weak signal features, product operators are the better choice.

3.6.2. Structuring Element Construction

Structuring element construction involves the definition of three parameters: shape, length and height.

First, flat SE is discussed. In general, the shape almost has no effect on processing a 1D vibration signal. This is because of space dimension mismatching between structuring element and a given signal. In order to explain the problem, a diamond-shaped SE presented in Figure 5 is considered, in which a black dot and gray dot represent 1 and 0, respectively. The black one circled by a red rectangle is the origin. Let a 1D signal be $\{x_0, x_1, \ldots, x_i, \ldots, x_{n-1}, x_n\}$. When the point x_i is processed and firstly overlapped with the origin, these points only at the left and right sides of x_i can be introduced into the morphological operation, because there are no others at the top and bottom area of x_i. It demonstrates that the complex shape has influence on a one-dimensional signal processed by morphological operations. Subsequently, the length is only defined. It corresponds to the selection of the temporal scale in signal analysis in essence. Due to the nonlinear and modulation of the vibrations of rotating parts faults, the length should match with the time scale of the minimum resolvable physical feature within the signal. For example, it should be slightly bigger than the duration of an impulse produced by rotating parts faults for surpass high-frequency noise. On the other hand, it should be shorter than the period of characteristic signals, so as to avoid distorting the modulation structure and its sideband information of signals.

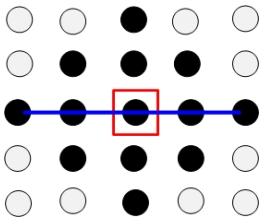


Figure 5. Dimond structuring element. The red box is the original of SE, and the dots linked by blue are effective elements for one-dimensional analysis.

To a non-flat SE, the definitions of the three parameters should directly reflect the characteristics of transient impacts and modulated envelops of vibration signals. The SE shape should match with the morphological features of an impulse produced by rotating part faults. In this case, sinusoidal, sinusoid and bell-shaped can be a candidate, with better matching with the concentration of transient energy. The definition of the length of non-flat SE is the same as that of the flat SE mentioned above. The height of the SE corresponds to the magnitude of the impact or the energy level of the fault, thereby enhancing fault-

modulated components while avoiding excessive amplification of noise. When diagnosing the rotating part defects of multi-source coupling and overlapping modulation, multi-scale and multi-shape non-flat SEs can be adopted.

Generally speaking, to flat or non-flat structure element, their physical properties can represent morphological features of a signal in both time and spatial domains. This allows mathematical morphology to fully use its nonlinear filtering ability and shape-matching characteristics, thus theoretically enhancing the effectiveness and reliability of rotating part fault diagnosis.

3.7. Comparison and Analysis of Four Methods in Applications

Aiming at rotating part fault diagnosis, four methods based on MM are introduced, i.e., single-scale mathematical morphology, multiple-scale mathematical morphology, morphological pattern spectrum and morphological wavelet. In order to understand the four methods in actual applications, the comparison and analyses across them are presented as follows:

(1) Noise Robustness. SSM highly depends on the length and height scale of SE, and only one SE match with the morphological feature of a signal in one scale; thus, its noise robustness is lowest among the four methods. MSM uses structuring elements with various scales, which can effectively inhibit random noise. Relatively speaking, the noise robustness of MSM is moderate but stronger than that of SSM. MPS is a multi-scale quantitative analysis, and can suppress noise interference through global morphological distribution; thus, it has strong noise robustness. MW fully takes advantage of morphological nonlinear filtering and wavelet multiresolution analysis, while simultaneously suppressing transient noise and background noise. Accordingly, it has the strongest noise robustness.

(2) Computational Cost and Real-Time Applicability. Obviously, computational cost is positively correlated with time complexity; thus, the order is SSM < MSM < MW < MPS. Firstly, SSM just completes one basic morphological operation, and the time complexity is O(N) (N is the number of sampling points). When MSM is conducted, all scales are involved into morphological operations, and its complexity is O(KN) (K is the number of scales). MW is the combination of morphology operation and wavelet transform, and the time complexity is O(NlogN). MPS requires performing multi-scale morphology operations and then quantifying the distribution of signal features. Therefore, the complexity is O(KN + NlongN). Based on the order of computational cost, the real-time applicability is an inverse order.

(3) Parameter Sensitivity. SSM heavily relies on the physical properties of single SE, and if these properties are unreasonable, it results in feature loss or distortion in the time domain. Hence, it has the highest parameter sensitivity across the four methods. MSM requires optimizing the number of scales and their related parameters, and sensitivity is moderate. MPS is affected by the scale range, but the pattern spectrum distribution performance further impairs the interference of single parameter, so its sensitivity is lower than that of MSM. MW simultaneously considers the number of the SE scales and the level of wavelet decomposition, but its sensitivity is lower than that of SSM.

(4) Suitability for Incipient Faults. It depends on the ability of a method to capture weak fault signatures. SSM struggles to balance noise suppression with weak feature preservation, in fact, it is easily masked by strong background signals. As a result, it is unable to extract such weak signal features. Differently, MSM can improve weak feature signal extraction through multi-scale screening; thus, its suitability is stronger when compared with SSM. MPS is based on MSM, and on this point, the suitability of MPS is almost the same as that of MSM. MW combines the advantages of both

MM and wavelet transform, so it can effectively capture the faint transient impacts of incipient rotating part faults while removing background noise in different frequency bands. Consequently, the morphological wavelet has the strongest suitability among the four methods.

According to the above description, the four methods show distinct performance in rotating part fault detection. Overall, method choosing should comprehensively consider the five aspects, thereby balancing diagnostic performance with the actual requirement.

4. Discussion and Development Orientation

Under the framework of mathematical morphology, four methods are introduced and their relevant applications on detecting rotating machine flaws are presented in this study. As an open study topic, several potential developments in mathematical morphology are suggested as follows:

(1) When single- and multi-scale analyses are performed using SE, especially Large-scale ones, it easily suffers from edge distortion in the time domain due to the nonlinear filtering mechanism, i.e., local extrema search. So, considering both restoring signal in time domain and keeping this nonlinear filtering, how to alleviate the time-domain distortion as much as possible should be further studied.

(2) In morphology theory, the core is how to construct the structure element adaptively. It can be known that once the scales are defined, they will not change in morphological operations. However, dynamic characteristics of a real signal always change. Obviously, if the definition of SE can match with the change, it relieves the dependence to the scale constraint, highlighting the dynamic characteristics of a signal, and enhancing the feature extracting capacity.

(3) One of the advantages of morphology is its relatively low computation cost, and it is very essential to real-time monitoring of mechanical equipment. We notice that the shifting of SE inside an original signal adopts the point-wise model, but sometimes it is maybe unnecessary for such processing, at least in specific range; for example, the interval between two impulses produced by rotating part faults. In a permissible condition that the feature information in time- or frequency-domain has no loss, the non-pointwise shifting could be considered, and it can further improve the morphology computation efficiency.

(4) Morphology pattern spectrum is a fault classification tool. In practice, noise disturbance will affect this processing accuracy, and MPS is the moment of the first order of a distribution function. On the other hand, in the mechanical fault diagnosis area, the noisy signal is defined as Gaussian white noise, and relevant studies have found that compared to lower-order statistics, higher-order statistics exhibit a better effect in suppressing such noise [177,178]. As a result, it could be used in the applications of MPS, thereby enhancing feature shape classification performance.

(5) Nonlinear multiresolution morphological wavelets rely on predefined morphological operators and scale parameters, lacking a systematic function space theory and completeness proofs. As a result, it is necessary to establish an intrinsic nonlinear multiresolution analysis framework, strictly defining their approximation and regularity properties. It would be useful for scale selection and optimal decomposition.

(6) Morphology processing is conducted through a single computation in single-scale morphology and through multiple computations in MSM, MPS and MW. However, these computations are largely independent of each other, indicating that the methods highly rely on the predefined SE. If a novel computation model can be developed, the dependence to SE might be reduced to some extent. On the other hand, the gradient descent algorithm in optimization theory iteratively converges to the optimal solution. For instance, Ref. [91] proposed an iterative mathematical morphology, where a unit-scale flat SE is

simply defined. The specific model indeed alleviates the dependence to SE. Accordingly, if a novel morphology method can be designed, it could be a valuable reference advancing mathematical morphology.

5. Concluding Remarks

A literature summarization on mathematical morphology and actual applications in rotating machine fault diagnosis is presented in this paper. Section 2 describes structuring elements, morphology operators and four morphology-based methods: single-scale morphology, multi-scale morphology, morphological pattern spectrum and morphological wavelet. Their typical applications on rotating machine fault diagnosis and classification are given in Section 3, with a clear classification as fault object and diagnostic methods. Meanwhile, this section gives the general rules of the operator selection and the SE construction, and the comparative analysis of four methods in noise robustness, computational cost, parameter sensitivity, suitability for incipient faults, and real-time applicability. Finally, several potential research directions are proposed. This review paper aims to systematically present the diagnosis methods based on mathematical morphology and to summarize their applications in the rotatory machine fault detection field. It is intended to serve as a comprehensive reference to researchers interested in mathematical morphology for rotating machine fault diagnosis.

Author Contributions: Methodology, writing—original draft, T.G.; writing—review and editing, supervision, X.Y. and Z.L.; literature investigation and formal analysis, B.J. All authors have read and agreed to the published version of the manuscript.

Funding: This work was supported by National Natural Science Foundation of China (No. U1765201, No. 41571514).

Data Availability Statement: The original contributions presented in this study are included in the article. Further inquiries can be directed to the corresponding author.

Conflicts of Interest: The authors declare that they have no known competing financial interests or personal relationships that could have appeared to influence the work reported in this paper.

References

1. Jardine, A.K.S.; Lin, D.; Banjevic, D. A Review on Machinery Diagnostics and Prognostics Implementing Condition-Based Maintenance. *Mech. Syst. Signal Proc.* **2006**, *20*, 1483–1510. [CrossRef]
2. Wei, Y.; Li, Y.; Xu, M.; Huang, W. A Review of Early Fault Diagnosis Approaches and Their Applications in Rotating Machinery. *Entropy* **2019**, *21*, 409. [CrossRef] [PubMed]
3. Griffin, D.; Lim, J. Signal Estimation from Modified Short-Time Fourier Transform. *IEEE Trans. Acoust. Speech Signal Process.* **1984**, *32*, 236–243. [CrossRef]
4. Durak, L.; Arikan, O. Short-Time Fourier Transform: Two Fundamental Properties and an Optimal Implementation. *IEEE Trans. Signal Process.* **2003**, *51*, 1231–1242. [CrossRef]
5. Sun, R.-B.; Yang, Z.; Chen, X.; Tian, S.; Xie, Y. Gear Fault Diagnosis Based on the Structured Sparsity Time-Frequency Analysis. *Mech. Syst. Signal Proc.* **2018**, *102*, 346–363. [CrossRef]
6. Liu, H.; Li, L.; Ma, J. Rolling Bearing Fault Diagnosis Based on STFT-Deep Learning and Sound Signals. *Shock Vib.* **2016**, *2016*, 1–12. [CrossRef]
7. Tao, H.; Wang, P.; Chen, Y.; Stojanovic, V.; Yang, H. An Unsupervised Fault Diagnosis Method for Rolling Bearing Using STFT and Generative Neural Networks. *J. Frankl.* **2020**, *357*, 7286–7307. [CrossRef]
8. Yan, R.; Gao, R.X.; Chen, X. Wavelets for Fault Diagnosis of Rotary Machines: A Review with Applications. *Signal Process.* **2014**, *96*, 1–15. [CrossRef]
9. Yuan, J.; Yao, Z.; Zhao, Q.; Xu, Y.; Li, C.; Jiang, H. Dual-Core Denoised Synchrosqueezing Wavelet Transform for Gear Fault Detection. *IEEE Trans. Instrum. Meas.* **2021**, *70*, 3521611. [CrossRef]
10. Fan, X.; Zuo, M.J. Gearbox Fault Detection Using Hilbert and Wavelet Packet Transform. *Mech. Syst. Signal Proc.* **2006**, *20*, 966–982. [CrossRef]

11. Sung, C.K.; Tai, H.M.; Chen, C.W. Locating Defects of a Gear System by the Technique of Wavelet Transform. *Mech. Mach. Theory* **2000**, *35*, 1169–1182. [CrossRef]
12. Shao, H.; Jiang, H.; Wang, F.; Wang, Y. Rolling Bearing Fault Diagnosis Using Adaptive Deep Belief Network with Dual-Tree Complex Wavelet Packet. *ISA Trans.* **2017**, *69*, 187–201. [CrossRef] [PubMed]
13. Yu, D.; Cheng, J.; Yang, Y. Application of EMD Method and Hilbert Spectrum to the Fault Diagnosis of Roller Bearings. *Mech. Syst. Signal Process.* **2005**, *19*, 259–270. [CrossRef]
14. Yu, Y.; Yu, D.; Chen, J. A Roller Bearing Fault Diagnosis Method Based on EMD Energy Entropy and ANN. *Mech. Syst. Signal Proc.* **2006**, *294*, 269–277. [CrossRef]
15. Gong, X.; Ding, L.; Du, W.; Wang, H. Gear Fault Diagnosis Using Dual Channel Data Fusion and EEMD Method. *J. Sound Vib.* **2017**, *174*, 918–926. [CrossRef]
16. Wang, X.; Liu, C.; Bi, F.; Bi, X.; Shao, K. Fault Diagnosis of Diesel Engine Based on Adaptive Wavelet Packets and EEMD-Fractal Dimension. *Mech. Syst. Signal Proc.* **2013**, *41*, 581–597. [CrossRef]
17. Fu, Q.; Jing, B.; He, P.; Si, S.; Wang, Y. Fault Feature Selection and Diagnosis of Rolling Bearings Based on EEMD and Optimized Elman_AdaBoost Algorithm. *IEEE Sen. J.* **2018**, *18*, 5024–5034. [CrossRef]
18. Dragomiretskiy, K.; Zosso, D. Variational Mode Decomposition. *IEEE Trans. Signal Process.* **2014**, *62*, 531–544. [CrossRef]
19. Gong, T.; Yuan, X.; Yuan, Y.; Lei, X.; Wang, X. Application of Tentative Variational Mode Decomposition in Fault Feature Detection of Rolling Element Bearing. *Measurement* **2018**, *135*, 481–492. [CrossRef]
20. Liu, C.; Cheng, G.; Chen, X.; Pang, Y. Planetary Gears Feature Extraction and Fault Diagnosis Method Based on VMD and CNN. *Sensors* **2018**, *18*, 1523. [CrossRef]
21. Li, H.; Liu, T.; Wu, X.; Chen, Q. An Optimized VMD Method and Its Applications in Bearing Fault Diagnosis. *Measurement* **2020**, *166*, 108185. [CrossRef]
22. Zhou, J.; Xiao, M.; Niu, Y.; Ji, G. Rolling Bearing Fault Diagnosis Based on WGWOA-VMD-SVM. *Sensors* **2022**, *22*, 6281. [CrossRef] [PubMed]
23. Wang, Y.; Markert, R. Filter Bank Property of Variational Mode Decomposition and Its Applications. *Signal Process.* **2016**, *120*, 509–521. [CrossRef]
24. Serra, J. Introduction to Mathematical Morphology. *Graph. Models* **1986**, *35*, 283–305. [CrossRef]
25. Haralick, R.M.; Sternberg, S.R.; Zhuang, X. Image Analysis Using Mathematical Morphology. *IEEE Trans. Pattern Anal. Mach. Intell.* **1987**, *PAMI-9*, 532–550. [CrossRef]
26. Image Analysis and Mathematical Morphology. *Comput. Graph. Image Process.* **1982**, *20*, 96–97. [CrossRef]
27. Zana, F.; Klein, J.-C. Segmentation of Vessel-like Patterns Using Mathematical Morphology and Curvature Evaluation. *IEEE Trans. Image Process.* **2001**, *10*, 1010–1019. [CrossRef]
28. Shih, H.C.; Liu, E.-R. Automatic Reference Color Selection for Adaptive Mathematical Morphology and Application in Image Segmentation. *IEEE Trans. Image Process.* **2016**, *25*, 4665–4676. [CrossRef]
29. Bouchet, A.; Montes, S.; Ballarin, V.; Díaz, I. Intuitionistic Fuzzy Set and Fuzzy Mathematical Morphology Applied to Color Leukocytes Segmentation. *Signal Image Video Process.* **2019**, *14*, 557–564. [CrossRef]
30. Vincent, L.; Dougherty, E.R. Morphological Segmentation for Textures and Particles. In *Digital Image Processing Methods*; CRC Press: Boca Raton, FL, USA, 2020; pp. 43–102.
31. Wu, Y.; Li, Q. The Algorithm of Watershed Color Image Segmentation Based on Morphological Gradient. *Sensors* **2022**, *22*, 8202. [CrossRef]
32. Chatterjee, S.; Dey, D.; Munshi, S. Mathematical Morphology Aided Shape, Texture and Colour Feature Extraction from Skin Lesion for Identification of Malignant Melanoma. In Proceedings of the 2015 International Conference on Condition Assessment Techniques in Electrical Systems (CATCON), Bangalore, India, 10–12 December 2015; pp. 200–203.
33. Godse, R.; Bhat, S. Mathematical Morphology-Based Feature-Extraction Technique for Detection and Classification of Faults on Power Transmission Line. *IEEE Access* **2020**, *8*, 38459–38471. [CrossRef]
34. Xiong, W.; Zhou, L.; Yue, L.; Li, L.; Wang, S. An Enhanced Binarization Framework for Degraded Historical Document Images. *EURASIP J. Image Video Process.* **2021**, *2021*, 13. [CrossRef]
35. Kimori, Y. Mathematical Morphology-Based Approach to the Enhancement of Morphological Features in Medical Images. *J. Clin. Bioinform.* **2011**, *1*, 33. [CrossRef] [PubMed]
36. Moslem, O.S.; Foucher, S.; Lepage, R. River Extraction from High-Resolution SAR Images Combining a Structural Feature Set and Mathematical Morphology. *IEEE J. Sel. Top. Appl. Earth Observ. Remote Sens.* **2017**, *10*, 1025–1038.
37. Gavankar, N.L.; Ghosh, S.K. Automatic Building Footprint Extraction from High-Resolution Satellite Image Using Mathematical Morphology. *Eur. J. Remote Sens.* **2017**, *51*, 182–193. [CrossRef]
38. Ma, X.; Liu, S.; Hu, S.; Geng, P.; Liu, M.; Zhao, J. SAR Image Edge Detection via Sparse Representation. *Soft Comput.* **2017**, *22*, 2507–2515. [CrossRef]

39. Pei, Y.; Liu, C.; Lou, R. Multi-Scale Edge Detection Method for Potential Field Data Based on Two-Dimensional Variation Mode Decomposition and Mathematical Morphology. *IEEE Access* **2020**, *8*, 161138–161156. [CrossRef]
40. Zhao, Y.; Gui, W.; Chen, Z.; Tang, J.; Li, L. Medical Images Edge Detection Based on Mathematical Morphology. *IEEE Annu. Santa Barbar.* **2005**, *2005*, 6492–6495.
41. Huang, C.P.; Wang, R.Z. An Integrated Edge Detection Method Using Mathematical Morphology. *Pattern Recogn, Image Anal.* **2006**, *16*, 406–412. [CrossRef]
42. Xu, M.K.; Ping, X.J.; Li, T.Y. A New Time-Frequency Spectrogram Analysis of FH Signals by Image Enhancement and Mathematical Morphology. In Proceedings of the Fourth International Conference Image and Graph, Chengdu, China, 22–24 August 2007; pp. 610–615.
43. Román, J.C.M.; Fretes, V.R.; Adorno, C.G.; Silva, R.G.; Noguera, J.L.V.; Legal-Ayala, H.; Mello-Román, J.D.; Torres, R.D.E.; Facon, J. Panoramic Dental Radiography Image Enhancement Using Multiscale Mathematical Morphology. *Sensors* **2021**, *21*, 3110. [CrossRef]
44. Maragos, P.; Pessoa, L.F. Morphological Filtering for Image Enhancement and Detection. In *The Image and Video Process Handbook*; Academic Press: San Diego, CA, USA, 1999; pp. 135–156.
45. Kimori, Y. Morphological Image Processing for Quantitative Shape Analysis of Biomedical Structures: Effective Contrast Enhancement. *J. Synchrot. Radiat.* **2013**, *20*, 848–853. [CrossRef] [PubMed]
46. Li, Q.; Qi, Y.S.; Gao, X.-J.; Li, Y.-T.; Liu, L.-Q. A Signal Based "W" Structural Elements for Multi-Scale Mathematical Morphology Analysis and Application to Fault Diagnosis of Rolling Bearings of Wind Turbines. *Int. J. Autom. Comput.* **2021**, *18*, 993–1006. [CrossRef]
47. Hu, A.J.; Tang, G.J.; An, L.S. New Method of Removing Pulsed Noises in Vibration Data. *J. Vib. Shock.* **2006**, *25*, 126−129.
48. Zhang, W.; Zhou, X.; Lin, Y. Application of Morphological Filter in Pulse Noise Removing of Vibration Signal. In Proceedings of the Congress on Image and Signal Processing, Sanya, China, 27–30 May 2008; pp. 132–135.
49. Maragos, P. Pattern Spectrum and Multiscale Shape Representation. *IEEE Trans. Pattern Anal. Mach. Intell.* **1989**, *11*, 701–716. [CrossRef]
50. Matheron, G. *Random Sets and Integral Geometry*; John Wiley & Sons: Hoboken, NJ, USA, 1974.
51. Dornaika, F.; Zhang, H. Granulometry Using Mathematical Morphology and Motion. In Proceedings of the IAPR Machine Vision Applications, Tokyo, Japan, 28–30 November 2000; pp. 51–54.
52. Maria, V.; Vitria, J.M. Mathematical Morphology, Granulometries, and Texture Perception. In Proceedings of the SPIE Conference Image Algebra Morphological Image Processing IV, San Diego, CA, USA, 23 June 1993; pp. 152–161.
53. Laurent, N.; Talbot, H. *Mathematical Morphology: From Theory to Applications*; John Wiley & Sons: Hoboken, NJ, USA, 2013.
54. Serra, J.; Soille, P. *Mathematical Morphology and Its Applications to Image Processing*; Springer Science & Business Media: Berlin/Heidelberg, Germany, 2012.
55. Pei, S.-C. Subband Decomposition of Monochrome and Color Images by Mathematical Morphology. *Opt. Eng.* **1991**, *30*, 921. [CrossRef]
56. Pei, S.-C.; Chen, F.-C. Hierarchical Image Representation by Mathematical Morphology Subband Decomposition. *Pattern Recognit. Lett.* **1995**, *16*, 183–192. [CrossRef]
57. Egger, O.; Li, W. Very Low Bit Rate Image Coding Using Morphological Operators and Adaptive Decompositions. In Proceedings of the International Conference on Image Processing, Tustin, CA, USA, 13–16 November 1994; pp. 326–330.
58. Florêncio, D.A.F.; Schafer, R.W. A Non-Expansive Pyramidal Morphological Image Coder. In Proceedings of the International Conference on Image Processing, Austin, TX, USA, 13–16 November 1994; pp. 331–335.
59. de Queiroz, R.L.; Florencio, D.A.F.; Schafer, R.W. Nonexpansive Pyramid for Image Coding Using a Nonlinear Filterbank. *IEEE Trans. Image Process.* **1998**, *7*, 246–252. [CrossRef]
60. Cha, H.; Luis, F.C. Adaptive Morphological Representation of Signals: Polynomial and Wavelet Methods. *Multidimens. Syst. Signal Process.* **1997**, *8*, 249−271. [CrossRef]
61. Sweldens, W. The Lifting Scheme: A Construction of Second Generation Wavelets. *SIAM J. Math. Anal.* **1998**, *29*, 511–546. [CrossRef]
62. Sweldens, W. The Lifting Scheme: A Custom-Design Construction of Biorthogonal Wavelets. *Appl. Comput. Harmon. Anal.* **1996**, *3*, 186–200. [CrossRef]
63. Sweldens, W. Lifting Scheme: A New Philosophy in Biorthogonal Wavelet Constructions. In Proceedings of the Wavelet Applications Signal Image Processing III, San Diego, CA, USA, 12–14 July 1995; pp. 68–79.
64. Heijmans, H.J.A.M.; Goutsias, J. Nonlinear Multiresolution Signal Decomposition Schemes. II. Morphological Wavelets. *IEEE Trans. Image Process.* **2000**, *9*, 1897–1913. [CrossRef] [PubMed]
65. Goutsias, J.; Heijmans, H.J.A.M. Nonlinear Multiresolution Signal Decomposition Schemes. I. Morphological Pyramids. *IEEE Trans. Image Process.* **2000**, *9*, 1862–1876. [CrossRef] [PubMed]

66. Nikolaou, N.G.; Antoniadis, I.A. Application of morphological operators as envelope extractors for impulse-type periodic signals. *Mech. Syst. Signal Proc.* **2003**, *17*, 1147–1162. [CrossRef]
67. Huang, J.; Cui, L.; Zhang, J. Novel Morphological Scale Difference Filter with Application in Localization Diagnosis of Outer Raceway Defect in Rolling Bearings. *Mech. Mach. Theory* **2023**, *184*, 105288. [CrossRef]
68. Chen, X.; Liu, X.; Dong, S.; Liu, J. Single-Channel Bearing Vibration Signal Blind Source Separation Method Based on Morphological Filter and Optimal Matching Pursuit (MP) Algorithm. *J. Vib. Control* **2013**, *21*, 1757–1768. [CrossRef]
69. Jiang, C.; Liu, J.; Zhang, H.; Shi, K. A New Bearing Fault Diagnosis Scheme Using MED-Morphological Filter and Ridge Demodulation Analysis. *J. Vibroeng.* **2015**, *17*, 4231–4247.
70. Duan, R.; Liao, Y. Impulsive Feature Extraction with Improved Singular Spectrum Decomposition and Sparsity-Closing Morphological Analysis. *Mech. Syst. Signal Process.* **2022**, *180*, 109436. [CrossRef]
71. Meng, L.; Xiang, J.; Wang, Y.; Jiang, Y.; Gao, H. A Hybrid Fault Diagnosis Method Using Morphological Filter–Translation Invariant Wavelet and Improved Ensemble Empirical Mode Decomposition. *Mech. Syst. Signal Proc.* **2015**, *50–51*, 101–115. [CrossRef]
72. Yu, J.; Hu, T.; Liu, H. A New Morphological Filter for Fault Feature Extraction of Vibration Signals. *IEEE Access* **2019**, *7*, 53743–53753. [CrossRef]
73. Hu, Z.; Wang, C.; Zhu, J.; Liu, X.; Kong, F. Bearing Fault Diagnosis Based on an Improved Morphological Filter. *Measurement* **2015**, *80*, 163–178. [CrossRef]
74. Yan, X.; Jia, M. Application of CSA-VMD and Optimal Scale Morphological Slice Bispectrum in Enhancing Outer Race Fault Detection of Rolling Element Bearings. *Mech. Syst. Signal Proc.* **2019**, *122*, 56–86. [CrossRef]
75. Van, M.; Franciosa, P.; Ceglarek, D. Rolling Element Bearing Fault Diagnosis Using Integrated Nonlocal Means Denoising with Modified Morphology Filter Operators. *Math. Probl. Eng.* **2016**, *1*, 1–14. [CrossRef]
76. Liu, X.; Xu, Q.; Wei, D.; Bo, L. Bearing Compound-Fault Detection Using Group Sparse Balanced Morphological Filtering. *Measurement* **2026**, *258*, 119447. [CrossRef]
77. Zhou, H.; Yang, J.; Xiang, H.; Chen, J. An Adaptive Morphological Filtering and Feature Enhancement Method for Spindle Motor Bearing Fault Diagnosis. *Appl. Acoust.* **2023**, *209*, 109400. [CrossRef]
78. Li, Q.; Chen, B.; Zhang, W.; Song, D. Research on Mathematical Morphological Operators for Fault Diagnosis of Rolling Element Bearings. *Measurement* **2022**, *203*, 111964. [CrossRef]
79. Wang, S.; Mei, G.; Chen, B.; Cheng, Y.; Cheng, B. Fault Diagnosis of Rolling Bearings Based on Enhanced Optimal Morphological Gradient Product Filtering. *Measurement* **2022**, *196*, 111279. [CrossRef]
80. Zhang, X.; Kang, J.; Xiao, L.; Zhao, J. Alpha Stable Distribution Based Morphological Filter for Bearing and Gear Fault Diagnosis in Nuclear Power Plant. *Sci. Technol. Nucl. Install.* **2015**, *1*, 1–15. [CrossRef]
81. Wang, T.; Chen, C.; Luo, Y.; Huang, S. Research on Fault Detection of Rolling Bearings in Press Line by a New Morphological Filter Based on Diagonal Slice Spectrum Lifting. *Measurement* **2022**, *188*, 110385. [CrossRef]
82. Lv, J.; Yu, J. Average Combination Difference Morphological Filters for Fault Feature Extraction of Bearing. *Mech. Syst. Signal Proc.* **2017**, *100*, 827–845. [CrossRef]
83. Li, Y.; Zuo, M.J.; Chen, Y.; Feng, K. An Enhanced Morphology Gradient Product Filter for Bearing Fault Detection. *Mech. Syst. Signal Proc.* **2018**, *109*, 166–184. [CrossRef]
84. Li, Y.; Liang, X.; Zuo, M.J. Diagonal Slice Spectrum Assisted Optimal Scale Morphological Filter for Rolling Element Bearing Fault Diagnosis. *Mech. Syst. Signal Proc.* **2016**, *85*, 146–161. [CrossRef]
85. Feng, G.B.; Zhu, Y.-B.; Sun, H.-G. Study on Fault Diagnosis of Gearbox Based on Morphological Filter and Multi-Fractal Theory. In Proceedings of the International Conference on Quality, Reliability, Risk, Maintenance, and Safety Engineering, Xi'an, China, 17–19 June 2011; pp. 472–477.
86. Zhou, L. Application of Morphological Demodulation in Gear Fault Feature Extraction. *J. Zhejiang Univ. (Eng. Sci.)* **2010**, *44*, 1514–1518.
87. Yu, F.; Zhu, Y. Fault Diagnosis of Reducer Based on Dual-Tree Complex Wavelet Packet and Morphology. In Proceedings of the 2023 Global Reliability and Prognostics and Health Management Conference (PHM-Hangzhou), Hangzhou, China, 12 October 2023; pp. 1–4.
88. Bo, L.; Liu, X.; Qin, S. Hybrid wavelet-morphology-EMD analysis and its application. *J. Vib. Shock* **2008**, *27*, 1–4.
89. Guo, J.; Zhen, D.; Li, H.; Shi, Z.; Gu, F.; Ball, A. Fault Detection for Planetary Gearbox Based on an Enhanced Average Filter and Modulation Signal Bispectrum Analysis. *ISA Trans.* **2020**, *101*, 408–420. [CrossRef]
90. Feng, Y.; Lu, B.; Zhang, D. Multiscale Morphological Manifold for Rolling Bearing Fault Diagnosis. *Proc. Inst. Mech. Eng. Mech. Eng. Sci.* **2016**, *231*, 3516–3529. [CrossRef]
91. Gong, T.; Yuan, Y.; Yuan, X.; Wu, X. Application of Optimized Multiscale Mathematical Morphology for Bearing Fault Diagnosis. *Meas. Sci. Technol.* **2017**, *28*, 045401. [CrossRef]

92. Lv, C.; Zhang, P.; Wu, D.; Li, B.; Zhang, Y. Bearing Fault Signal Analysis Based on an Adaptive Multiscale Combined Morphological Filter. *Int. J. Rotating Mach.* **2020**, *1*, 1–8. [CrossRef]
93. Tang, M.; Liao, Y.; He, D.; Duan, R.; Zhang, X. Rolling Bearing Diagnosis Based on an Unbiased-Autocorrelation Morphological Filter Method. *Measurement* **2021**, *189*, 110617. [CrossRef]
94. Gong, T.; Yuan, Y.; Yuan, X.; Wang, X.; Wu, X.; Li, Y. Iterative Asymmetric Multiscale Morphology and Its Application to Fault Detection for Rolling Element Bearing. *Proc. Inst. Mech. Eng. Part C-J. Eng. Mech. Eng. Sci.* **2017**, *232*, 316–330. [CrossRef]
95. Li, Y.; Liang, X.; Lin, J.; Chen, Y.; Liu, J. Train Axle Bearing Fault Detection Using a Feature Selection Scheme Based Multi-Scale Morphological Filter. *Mech. Syst. Signal Proc.* **2018**, *101*, 435–448. [CrossRef]
96. Yan, X.; Tang, G.; Wang, X. A Chaotic Feature Extraction Based on SMMF and CMMFD for Early Fault Diagnosis of Rolling Bearing. *IEEE Access* **2020**, *8*, 179497–179515. [CrossRef]
97. Qu, X.; Zhang, Y.; Yin, L. Fault Diagnosis for Road Heading Bearings Based on a Multiscale Enhanced Cascaded Difference Filter. *J. Comput. Nonlinear Dyn.* **2024**, *19*, 031004. [CrossRef]
98. Yu, J.; Xiao, C.; Hu, T.; Gao, Y. Selective Weighted Multi-Scale Morphological Filter for Fault Feature Extraction of Rolling Bearings. *ISA Trans.* **2023**, *132*, 544–556. [CrossRef] [PubMed]
99. Li, Y.; Zuo, M.J.; Chen, Z.; Lin, J. Railway Bearing and Cardan Shaft Fault Diagnosis via an Improved Morphological Filter. *Health Monit.* **2019**, *19*, 1471–1486. [CrossRef]
100. Wang, Z.; Fan, J.; Guo, Y.; Chen, X.; Kang, W. Research on Fault Feature Extraction for Planet-Bearing Using Novel Combination Operator Morphological Filtering and Stochastic Resonance. *J. Sound Vib.* **2025**, *607*, 119037. [CrossRef]
101. Zhang, W.; Lu, H.; Zhang, Y.; Wang, Y.; Li, Z.; Yang, M.; Cui, Y. Enabling Accurate Detection and Localization of Bearing Faults under Noise and Vibration. *Appl. Acoust.* **2025**, *233*, 110528. [CrossRef]
102. Li, Y.; Xu, M.; Liang, X.; Huang, W.-H. Application of Bandwidth EMD and Adaptive Multiscale Morphology Analysis for Incipient Fault Diagnosis of Rolling Bearings. *IEEE Trans. Ind. Electron.* **2017**, *64*, 6506–6517. [CrossRef]
103. Yao, R.; Guo, C.; Deng, W.; Zhao, H. A Novel Mathematical Morphology Spectrum Entropy Based on Scale-Adaptive Techniques. *ISA Trans.* **2022**, *126*, 691–702. [CrossRef]
104. Shuai, J.; Shen, C.; Zhu, Z. Adaptive Morphological Feature Extraction and Support Vector Regressive Classification for Bearing Fault Diagnosis. *Int. J. Rotating Mach.* **2017**, *1*, 1–10. [CrossRef]
105. Cui, L.; Wang, J.; Ma, J. Early Fault Detection Method for Rolling Bearing Based on Multiscale Morphological Filtering of Information-Entropy Threshold. *J. Mech. Sci. Technol.* **2019**, *33*, 1513–1522. [CrossRef]
106. Duan, R.; Liao, Y.; Yang, L.; Xue, J.; Tang, M. Minimum Entropy Morphological Deconvolution and Its Application in Bearing Fault Diagnosis. *Measurement* **2021**, *182*, 109649. [CrossRef]
107. Tang, M.; Liao, Y.; Duan, R.; Xue, J.; Zhang, X. Bearing Fault Diagnosis Based on the Maximum Squared-Enveloped Multipoint Kurtosis Morphological Deconvolution. *IEEE Trans. Instrum. Meas.* **2022**, *71*, 3509711. [CrossRef]
108. Deng, F.; Yang, S.; Tang, G.; Hao, R.; Zhang, M. Self Adaptive Multi-Scale Morphology AVG-Hat Filter and Its Application to Fault Feature Extraction for Wheel Bearing. *Meas. Sci. Technol.* **2017**, *28*, 045011. [CrossRef]
109. Yan, X.; Liu, T.; Fu, M.; Ye, M.; Jia, M. Bearing Fault Feature Extraction Method Based on Enhanced Differential Product Weighted Morphological Filtering. *Sensors* **2022**, *22*, 6184. [CrossRef]
110. Wang, S.; Chen, B.; Cheng, Y.; Jiang, X. Investigation on Morphological Filtering via Enhanced Adaptive Time-Varying Structural Element for Bearing Fault Diagnosis. *Measurement* **2025**, *244*, 116466. [CrossRef]
111. Wang, S.; Mei, G.; Chen, B.; Cheng, Y. An Improved Time-Varying Morphological Filtering and Its Application to Bearing Fault Diagnosis. *IEEE Sens. J.* **2022**, *22*, 20707–20717. [CrossRef]
112. Ye, Z.; Yue, S.; Yang, P.; Zhou, R.; Yu, J. Deep Morphological Shrinkage Convolutional Autoencoder-Based Feature Learning of Vibration Signals for Gearbox Fault Diagnosis. *IEEE Trans. Instrum. Meas.* **2024**, *73*, 3510712. [CrossRef]
113. Ye, Z.; Yu, J. Multiscale Weighted Morphological Network Based Feature Learning of Vibration Signals for Machinery Fault Diagnosis. *IEEE/ASME Trans. Mechatron.* **2022**, *27*, 1692–1703. [CrossRef]
114. Guo, J.C.; Shi, Z.Q.; Li, H.Y.; He, Z.J. Transient Impulses Enhancement Based on Adaptive Multi-Scale Improved Differential Filter and Its Application in Rotating Machines Fault Diagnosis. *ISA Trans.* **2022**, *120*, 271–292. [CrossRef]
115. Wang, J.; Wang, H.; Guo, L.; Yang, D. Modeling and Fault Identification of the Gear Tooth Surface Wear Failure System. *Int. J. Nonlinear Sci. Numer. Simul.* **2021**, *22*, 341–351. [CrossRef]
116. Cai, J.H.; Li, X.Q. Gear Fault Diagnosis Based on Time–Frequency Domain De-Noising Using the Generalized S Transform. *J. Vib. Control* **2018**, *24*, 3338–3347. [CrossRef]
117. Li, Y.B.; Li, G.Y.; Yang, Y.T.; Liang, X.H.; Xu, M.Q. A Fault Diagnosis Scheme for Planetary Gearboxes Using Adaptive Multi-Scale Morphology Filter and Modified Hierarchical Permutation Entropy. *Mech. Syst. Signal Proc.* **2018**, *105*, 319–337. [CrossRef]
118. Wei, Y.; Xu, M.; Wang, X.; Huang, W.; Li, Y. A Hybrid Approach for Weak Fault Feature Extraction of Gearbox. *IEEE Access.* **2019**, *7*, 16616–16625. [CrossRef]

119. Luo, J.S.; Yu, D.J.; Liang, M. Gear Fault Detection under Time-Varying Rotating Speed via Joint Application of Multiscale Chirplet Path Pursuit and Multiscale Morphology Analysis. *Struct. Health Monit.* **2012**, *11*, 526–537. [CrossRef]
120. Zhang, L.; Zhang, L.; Yang, J.; Li, M. Adaptive Morphological Filter to Fault Diagnosis of Gearbox. In Proceedings of the International Conference on Consumer Electronics, Communications and Networks, Xianning, China, 6–18 April 2011; pp. 70–73.
121. Yu, J.B.; Huang, J.H.; Liu, C.H.; Li, Z.N.; Chen, B.Q. Fault Feature of Gearbox Vibration Signals Based on Morphological Filter Dynamic Convolution Autoencoder. *IEEE Sens. J.* **2022**, *22*, 22931–22942. [CrossRef]
122. Liu, T.T.; Cui, L.L.; Zhang, C. Study on Fault Diagnosis Method of Planetary Gearbox Based on Turn Domain Resampling and Variable Multi-Scale Morphological Filtering. *Symmetry* **2021**, *13*, 52. [CrossRef]
123. Yan, X.; She, D.; Xu, Y.; Jia, M. Application of Generalized Composite Multiscale Lempel–Ziv Complexity in Identifying Wind Turbine Gearbox Faults. *Entropy* **2021**, *23*, 1372. [CrossRef]
124. Liu, T.T.; Cui, L.L.; Zhang, J.Y.; Li, G. Research on Fault Diagnosis of Planetary Gearbox Based on Variable Multi-Scale Morphological Filtering and Improved Symbol Dynamic Entropy. *Int. J. Adv. Manuf. Technol.* **2023**, *124*, 3947–3961. [CrossRef]
125. Zhuang, Y.; Yu, J.B. Deep Morphological Convolutional Network for Feature Learning of Vibration Signals and Its Applications to Gearbox Fault Diagnosis. *Mech. Syst. Signal Proc.* **2021**, *161*, 107984.
126. Cao, S.X.; Li, H.K.; Zhang, K.L.; Zhang, Y.; Li, Y.F. Strategy for Detection and Suppression of Random Impulse Interferences in Gearbox Vibration Signals. *IEEE Sens.* **2024**, *24*, 3523–3539. [CrossRef]
127. Chen, Q.; Chen, Z.W.; Sun, W.; Li, C.S. A New Structuring Element for Multi-Scale Morphology Analysis and Its Application in Rolling Element Bearing Fault Diagnosis. *J. Vib. Control* **2015**, *21*, 765–789. [CrossRef]
128. Gao, J.W.; Wang, R.C.; Zhang, R.L.; Li, H.F.; Li, H.B. A Novel Fault Diagnosis Method for Rotating Machinery Based on S Transform and Morphological Pattern Spectrum. *J. Braz. Soc. Mech. Sci. Eng.* **2016**, *38*, 1575–1584. [CrossRef]
129. Sun, D.; Wang, B.; Hu, X.; He, Q.B. A Fault Diagnosis Method Based on Improved Pattern Spectrum and FOASVM. *In. J. Acous. Vib.* **2019**, *24*, 312–319.
130. Zhu, W.Y.; Zhang, W.X.; Zhang, C. Rolling Bearing Fault Diagnosis Based on Mathematical Morphological Spectrum. *Mech. Mach. Sci.* **2023**, *129*, 688–698.
131. Li, Y.F.; Zuo, M.J.; Li, Y.B. Application of Modified Morphological Pattern Spectrum and LSSVM for Fault Diagnosis of Train Wheelset Bearings. In Proceedings of the International Conference on Sensing, Diagnostics, Prognostics, and Control, Xi'an, China, 15–17 August 2018; pp. 50–55.
132. Gao, J.; Tao, L.; Zhang, M.; Wang, R.C. New Time-Frequency Representations Based on the Morphological Pattern Spectrum for Bearing Fault Diagnosis. In Proceedings of the 7th International Conference on Computational Methods, Berkeley, CA, USA, 1–4 August 2016; pp. 213–231.
133. Hao, R.J.; Peng, Z.K.; Feng, Z.P.; Zhang, X.H.; Chu, F.L. Application of Support Vector Machine Based on Pattern Spectrum Entropy in Fault Diagnostics of Rolling Element Bearings. *Meas. Sci. Technol.* **2011**, *22*, 045708. [CrossRef]
134. Hao, R.J.; Feng, Z.P.; Chu, F.L. Defects Diagnosis and Classification for Rolling Bearing Based on Mathematical Morphology. In Proceedings of the 8th International Conference on Reliability, Maintainability and Safety, Chengdu, China, 20–24 July 2009; pp. 817–821.
135. Wang, W.J.; Cui, L.L.; Chen, D.Y. Multi-Scale Morphology Analysis of Acoustic Emission Signal and Quantitative Diagnosis for Bearing Fault. *Acta Mech. Sin.* **2016**, *32*, 265–272. [CrossRef]
136. Yu, X.T.; Lu, W.X.; Chu, F.L. Fault Diagnostics Based on Pattern Spectrum Entropy and Proximal Support Vector Machine. *Key Eng. Mater.* **2009**, *413*, 607–612. [CrossRef]
137. Yan, X.; Liu, Y.; Ding, P.; Jia, M.P.; Li, Y.B. Fault Diagnosis of Rolling-Element Bearing Using Multiscale Pattern Gradient Spectrum Entropy Coupled with Laplacian Score. *Complexity* **2020**, *1*, 1–29. [CrossRef]
138. Zhao, H.M.; Yao, R.; Xu, L.; Yuan, Y.B.; Li, Y.B. Study on a Novel Fault Damage Degree Identification Method Using High-Order Differential Mathematical Morphology Gradient Spectrum Entropy. *Entropy* **2018**, *20*, 682. [CrossRef]
139. Zhao, H.M.; Liu, H.D.; Xu, J.J.; Li, Y.B. Performance Prediction Using High-Order Differential Mathematical Morphology Gradient Spectrum Entropy and Extreme Learning Machine. *IEEE Tran. Instrum. Meas.* **2020**, *69*, 4165–4172. [CrossRef]
140. Li, H.R.; Wang, Y.K.; Wang, B.; Luo, M.Y.; Li, Y.B. The Application of a General Mathematical Morphological Particle as a Novel Indicator for the Performance Degradation Assessment of a Bearing. *Mech. Syst. Signal Proc.* **2017**, *82*, 490–502. [CrossRef]
141. Gao, H.; Liu, J.; Li, Y. A New Approach for Performance Degradation Feature Extraction Based on Generalized Pattern Spectrum Entropy. *Proc. Inst. Mech. Eng. Part C-J. Mech. Eng. Sci.* **2015**, *231*, 1932–1945. [CrossRef]
142. Wang, B.; Wang, W.; Hou, M.H.; Li, H.R.; Li, Y.B. Bearing Performance Degradation Condition Recognition Based on a Combination of Improved Pattern Spectrum Entropy and Fuzzy C-Means. *J. Intell. Fuzzy Syst.* **2018**, *34*, 3681–3693. [CrossRef]
143. Li, B.; Gao, M.; Guo, Q.; Zhang, P.L.; Liu, D.S. Characterizing Vibration Signals Utilizing Morphological Pattern Spectrum for Gear Fault Diagnosis. In Proceedings of the 3rd International Conference on Mechatronics, Robotics and Automation, Shenyang, China, 20–21 April 2015; pp. 707–711.

144. Li, B.; Zhang, P.-L.; Wang, Z.-J.; Mi, S.-S.; Liu, D.-S. Application of S Transform and Morphological Pattern Spectrum for Gear Fault Diagnosis. *Proc. Inst. Mech. Eng. Part C-J. Eng. Mech. Eng. Sci.* **2011**, *225*, 2963–2972. [CrossRef]
145. Barbieri, N.; Barbieri, G.; Martins, B.; Sant'Ana, R.; De Lacerda De Oliveira, L. Analysis of Automotive Gearbox Faults Using Vibration Signal. *Mech. Syst. Signal Process.* **2019**, *129*, 148–163. [CrossRef]
146. Wang, S.; Zhou, J. Fault Diagnosis of Rolling Bearing Based on Lifting Morphological Wavelet and Ensemble Empirical Mode Decomposition. In Proceedings of the International Conference on Consumer Electronics, Communications and Networks, Xining, China, 11–13 March 2011; pp. 2229–2232.
147. Li, B.; Zhang, P.L.; Mi, S.S.; Liu, D.S.; Ren, Y.Q. An Adaptive Morphological Gradient Lifting Wavelet for Detecting Bearing Defects. *Mech. Syst. Signal Proc.* **2012**, *29*, 415–427. [CrossRef]
148. Li, C.; Liang, M.; Zhang, Y.; Hou, S. Multi-Scale Autocorrelation via Morphological Wavelet Slices for Rolling Element Bearing Fault Diagnosis. *Mech. Syst. Signal Proc.* **2012**, *31*, 428–446. [CrossRef]
149. Chen, Q.H.; Li, H.R.; Xu, B.H. An Improved Multi-Scale Morphological Undecimated Wavelet Method and Its Application in Rolling Bearing Fault Feature Extraction. *Appl. Mech. Mater.* **2013**, *380*, 1009–1013. [CrossRef]
150. Hao, R.; Chu, F. Morphological undecimated wavelet decomposition for fault diagnostics of rolling element bearings. *J. Sound Vib.* **2009**, *320*, 1164–1177. [CrossRef]
151. Meng, L.J.; Xiang, J.W.; Zhong, Y.T.; Wang, Y.Y. Fault Diagnosis of Rolling Bearing Based on Second Generation Wavelet Denoising and Morphological Filter. *J. Mech. Sci. Technol.* **2015**, *29*, 3121–3129. [CrossRef]
152. Khakipour, M.H.; Safavi, A.A.; Setoodeh, P. Bearing Fault Diagnosis with Morphological Gradient Wavelet. *J. Frankl. Inst.* **2016**, *354*, 2465–2476. [CrossRef]
153. Li, Y.; Liang, X.; Liu, W.; Wang, Y. Development of a Morphological Convolution Operator for Bearing Fault Detection. *J. Sound Vib.* **2018**, *421*, 220–233. [CrossRef]
154. Guo, J.; He, Q.; Zhen, D.; Gu, F.; Ball, A.D. An Iterative Morphological Difference Product Wavelet for Weak Fault Feature Extraction in Rolling Bearing Fault Diagnosis. *Struct. Health Monit.* **2022**, *2222*, 296–318. [CrossRef]
155. Li, Y.; Feng, K.; Chen, Y.; Chen, Z. Multioperator Morphological Undecimated Wavelet for Wheelset Bearing Compound Fault Detection. *IEEE Trans. Instrum. Meas.* **2023**, *72*, 7504612. [CrossRef]
156. Li, H.; Tan, Y.; Pu, Y. Rolling Bearing Fault Vibration Signal Denoising Based on Adaptive Morphological Wavelet Perona–Malik Filter Algorithm. *Shock Vib.* **2021**, *2021*, 5575497. [CrossRef]
157. Duan, R.; Liao, Y.; Yang, L.; Song, E. Faulty Bearing Signal Analysis with Empirical Morphological Undecimated Wavelet. *IEEE Trans. Instrum. Meas.* **2022**, *71*, 3508711. [CrossRef]
158. Wang, H.; Ji, X.; Wang, X.; Li, Z.-N. Fault Feature Extraction of Fan Bearing Based on Improved Mathematical Morphological Unsampled Wavelet. *Chin. Autom. Congress.* **2017**, *33*, 3188–3192.
159. Zhang, W.; Shen, L.; Li, J.; Cai, Q.; Wang, H. Morphological Undecimated Wavelet Decomposition for Fault Feature Extraction of Rolling Element Bearing. In Proceedings of the 2009 2nd International Congress on Image and Signal Processing, Tianjin, China, 17–19 October 2009; pp. 1–5.
160. Yong, L. Rolling Bearing Fault Diagnosis Based on Morphological Wavelet Theory and Bi-Spectrum Analysis. *J. Zhejiang Univ-Eng. Sci.* **2010**, *44*, 432–439.
161. Yang, X.; Zhou, X.; Zhang, W.; Yang, F.; Lin, Y. Rolling Bearing Fault Feature Extraction Based on Morphological Wavelet and S-Transform. *J. Zhejiang Univ-Eng. Sci.* **2010**, *44*, 2088–2092.
162. Liu, X.; Xu, G.; Ren, S.; Yang, M. The morphological gradient wavelet de-noising and S transform-based gear fault feature extraction algorithm. *Electron. Des. Eng.* **2012**, *20*, 79–82.
163. Li, B.; Zhang, P.; Mao, Q.; Mi, S.; Liu, P. Gear Fault Detection Using Adaptive Morphological Gradient Lifting Wavelet. *J. Vib. Control* **2012**, *19*, 1646–1657. [CrossRef]
164. Zhang, W.B.; Su, Y.P.; Zhou, Y.J.; Pu, Y.S. A New Intelligent Fault Recognition Method for Gearbox. *Adv. Mater. Res.* **2013**, *684*, 369–372. [CrossRef]
165. Hong, S.; Fang, J.S.; Bo, C.; Wei, Q. Research of Gear Fault Detection in Morphological Wavelet Domain. *J. Phys. Conf. Ser.* **2016**, *679*, 012035. [CrossRef]
166. Zhang, W.; Pu, Y.; Guo, D.; Jiang, J.; Yu, L.; Min, J. Application of Morphological Wavelet and Permutation Entropy in Gear Fault Recognition. *Evol. Intell.* **2020**, *15*, 2427–2436. [CrossRef]
167. Cai, J.; Wang, X. Crack Fault Diagnosis of Gear Based on Morphological Wavelet De-Noising. *J. Mech. Strength* **2015**, *37*, 398–402.
168. Ding, W.; Zhang, Z.; Yao, L.; Huang, J. Fault Recognition Method of Transmission Gear Based on Morphological Wavelet and Permutation Entropy. *J. Mech. Transm.* **2019**, *43*, 165–168.
169. Zhang, P.; Li, B.; Zhang, Y.; Mi, S.; Liu, D. Max-Lifting Morphological Wavelet Transform Based Gear Fault Feature Extraction. *Chin. J. Sci. Instrum.* **2010**, *31*, 2736–2741.

170. Tong, R.; Kang, J.; Li, B.; Sun, J. A Preprocessing Method for the Vibration Signal of Gear Based on MUDW and CK. In Proceedings of the 2017 9th International Conference on Modelling, Identification and Control (ICMIC), Kunming, China, 10–12 July 2017; pp. 680–686.
171. Shen, L.; Zhou, X.; Liu, L.; Yang, F. Application of Morphological Wavelet De-noising in Extracting Gear Fault Feature. *Trans. Chin. Soc. Agr. Mach.* **2010**, *41*, 217–221.
172. Li, Y.-F.; Zuo, M.; Feng, K.; Chen, Y.-J. Detection of Bearing Faults Using a Novel Adaptive Morphological Update Lifting Wavelet. *Chin. J. Mech. Eng.* **2017**, *30*, 1305–1313. [CrossRef]
173. Li, Y.; Zuo, M.J.; Lin, J.; Liu, J. Fault Detection Method for Railway Wheel Flat Using an Adaptive Multiscale Morphological Filter. *Mech. Syst. Signal Proc.* **2017**, *84*, 642–658. [CrossRef]
174. Jiang, W.; Zheng, Z.; Zhu, Y.; Li, Y. Demodulation for Hydraulic Pump Fault Signals Based on Local Mean Decomposition and Improved Adaptive Multiscale Morphology Analysis. *Mech. Syst. Signal Proc.* **2015**, *58–59*, 179–205. [CrossRef]
175. Li, B.; Mi, S.; Liu, P.; Wang, Z. Classification of Time-Frequency Representations Using Improved Morphological Pattern Spectrum for Engine Fault Diagnosis. *J. Sound Vib.* **2013**, *332*, 3329–3337. [CrossRef]
176. Qiu, Z.; Li, W.; Wang, D. Multi-Source Information Fusion Based Axial Piston Pump Fault Diagnosis Method under Dynamic Conditions. *Eng. Res. Express* **2025**, *7*, 015567. [CrossRef]
177. Mborah, C.; Ge, M. Enhancing manual P-phase arrival detection and automatic onset time picking in a noisy microseismic data in underground mines. *Int. J. Min. Sci. Technol.* **2018**, *28*, 691–699. [CrossRef]
178. Dong, X.T.; Li, Y.; Wu, N.; Tian, Y.N.; Yu, P.J. The S-STK/LTK algorithm for arrival time picking of microseismic signals. *J. Geophys. Eng.* **2018**, *15*, 1484–1492. [CrossRef]

Disclaimer/Publisher's Note: The statements, opinions and data contained in all publications are solely those of the individual author(s) and contributor(s) and not of MDPI and/or the editor(s). MDPI and/or the editor(s) disclaim responsibility for any injury to people or property resulting from any ideas, methods, instructions or products referred to in the content.